Clim. Past, 21, 465–487, 2025
https://doi.org/10.5194/cp-21-465-2025

Climate of the Past
Open Access
EGU

New age constraints for glacial terminations IV, III, and III.a based on western Mediterranean speleothem records

Judit Torner[1], Isabel Cacho[1], Heather Stoll[2], Ana Moreno[3], Joan O. Grimalt[4], Francisco J. Sierro[5], Joan J. Fornós[6], Hai Cheng[7], and R. Lawrence Edwards[8]

[1]GRC Geociències Marines, Dept. de Dinàmica de la Terra i de l'Oceà, Universitat de Barcelona, 08028 Barcelona, Spain
[2]Department of Earth Sciences, ETH Zürich, 8092 Zurich, Switzerland
[3]Departamento de Procesos Geoambientales y Cambio Global, 639/, CSIC, 50059 Zaragoza, Spain
[4]Institute of Environmental Assessment and Water Research (IDAEA-CSIC), 08034 Barcelona, Spain
[5]Departmento de Geologìa, Universidad de Salamanca, 37008 Salamanca, Spain
[6]Earth Sciences Research Group. Departament de Biologia, Universitat de les Illes Balears, 07122 Palma (Mallorca), Spain
[7]Institute of Global Environmental Change, University of Xi'an Jiaotong, Xi'an, 710049, China
[8]Department of Earth Sciences, University of Minnesota, Minneapolis, MN 55455, USA

Correspondence: Judit Torner (j.torner@ub.edu)

Received: 30 July 2024 – Discussion started: 14 August 2024
Revised: 27 November 2024 – Accepted: 10 December 2024 – Published: 14 February 2025

Abstract. The full understanding of climate feedbacks responsible for the amplification of deglaciations requires robust chronologies for these climate transitions, but in the case of marine records, radiocarbon chronologies are possible only for the last glacial termination. Although the assumed relationships between the marine isotopic record and the orbital parameters provide a first-order chronology for glacial terminations, an independent chronological control allows the relationships between orbital forcing and the climate response to be evaluated over multiple previous terminations. To assess this, we present geochemical records from the western Mediterranean, including two speleothems and one marine sediment core. The most notable speleothem, the so-called RAT, established a new long terrestrial climate record for this region, spanning Marine Isotope Stages from MIS 11 to MIS 7. Its absolute U / Th dates provide an exceptional chronology for the glacial terminations IV, III, and III.a. The onset of these three glacial terminations was marked by rapid δ^{18}O depletions, reflecting ocean freshening by ice melting, thus providing an excellent tie point for regional marine records also sensitive to such freshening. This is exemplified by new δ^{18}O data of the Ocean Drilling Program (ODP) 977 site from the Alboran Sea, where the speleothem chronology was employed to adjust its age model. The new chronologies reveal an earlier onset of the deglacial melting for the TIV and TIII.a that is in contrast to the generally accepted marine chronologies and indicates that the duration of these deglaciations was variable, with TIV being particularly longer (∼ 20 kyr). This study also supports that the onset of deglacial melting always occurred during a declining precession index, while a nonunique relation occurred with the obliquity parameter.

1 Introduction

Glacial–interglacial transitions exemplify the highest amplitude of climate changes along the Late Quaternary and involve intense and fast processes of ice sheet melting that led to rapid sea level rise (Past Interglacials Working Group of PAGES, 2016). Although the increasing Northern Hemisphere summer insolation (NHSI) is considered the main driver for deglaciations, internal feedbacks from the Earth's climate system were crucial to trigger glacial terminations (Cheng et al., 2009; Drysdale et al., 2009; Tzedakis et al., 2012; Barker and Knorr, 2021). The consequences of the insolation rise depended on the actual extent of the ice sheet build-up during the preceding glacial period, determining the main features of terminations (Tzedakis et al., 2017). Ice sheet instability and intense events of massive icebergs re-

leased into the North Atlantic, named Heinrich-like events, are considered characteristic features of deglaciation (Barker et al., 2015, 2019; Barker and Knorr, 2021; Hodell et al., 2013, 2023) and have been well-documented through ice-rafting debris (IRD) records in the North Atlantic (Hodell et al., 2008; Barker et al., 2011). The consequent North Atlantic freshening caused by ice melting became the trigger for powerful feedback processes inducing glacial terminations. The freshwater discharge allowed surface water stratification and provoked the displacement of the deep-water formation, disturbing the strength of the Atlantic Meridional Overturning Circulation (AMOC) (Rahmstorf, 2002). This, in turn, changed the interhemispheric heat transport, inducing a rapid cooling in the North Atlantic region, whereas Antarctica gradually warmed. The asymmetry in the hemispheric heat transport (the bipolar seesaw) and its influence on the atmospheric CO_2 rise was also a fundamental requirement for deglaciation to occur (Cheng et al., 2009; Barker et al., 2011, 2019; Barker and Knorr, 2021; Tzedakis et al., 2012). Thus, variations in the AMOC and greenhouse gases explain much of the variability in the global climate during deglaciations (Clark et al., 2012). In parallel to the weakening of the AMOC, albedo changes due to the reduction in the continental ice sheet extent operated as secondary internal feedback or amplifier. At the end of the deglaciation arises the characteristic abrupt warming that leads to the onset of interglacial periods, but the sea level highstand marking the interglacial conditions occurred systematically a few thousand years after the maximum in the NH summer insolation due to the slow response of the ice sheets to insolation (Past Interglacials Working Group of PAGES, 2016). Several warm marine isotopic substages are considered interglacial acmes or peaks of optimum climate conditions (i.e., the Marine Isotopic Stages (MISs) 7a–c, 7e, 9e, and 11c within them). However, temporal and geographical asynchronicities in the precise definition of their boundaries between marine and terrestrial records or even different proxies within the same archives pose a challenge to resolving the feedbacks acting in these transitional periods (Shackleton, 1969, 2003; Sánchez-Goñi et al., 1999). These feedbacks responsible for past deglacial warming can also play a role in the ongoing situation of climate change. The increase in atmospheric CO_2 due to anthropogenic emissions, the reduction in Earth albedo resulting from ice melting, and even the weakening of the AMOC are currently in operation (IPCC, 2023; Boers, 2021). Studying past glacial terminations provides unique examples for elucidating the role that these internal components of Earth's climate system had during past periods of global climate warming, providing a testing ground for better contextualizing current climate change.

Astronomically tuned marine sediment records provided fundamental information to understand the evolution of the continental ice sheets in the past. Globally averaged $\delta^{18}O$ stacks from benthic foraminifera, reflecting changes in ice sheet build-up and deep-ocean temperature, have provided a global chronological framework for correlating marine sediment sequences, and the marker is its global signal driven by changes in the ice sheet build-up (Imbrie et al., 1984; Martinson et al., 1987; Lisiecki and Raymo, 2005). However, the chronology applied to such stacks is based on the assumption of a stationary relationship between insolation and ice volume changes and does not account for suborbital climate influence in the time sequences of each glacial termination (Hodell et al., 2015). While also reflecting ice volume cycles, the seawater oxygen isotopic signal ($\delta^{18}O_{sw}$) from planktonic records can be overprinted by regional temperature or hydrographic changes, thus challenging its use as an isotopic chronostratigraphic tool (Rohling et al., 2015). Hence, orbitally dependent marine isotopic chronologies are limited in resolving precise age constriction of key climate periods, such as glacial–interglacial transitions, complicating any interpretation in terms of orbital forcing.

A growing number of studies uses absolute dating from speleothems to anchor the marine records and achieve astronomically independent age models (e.g., Grant et al., 2012; Cheng et al., 2016). Speleothems with a relatively unambiguous climatic interpretation of their proxies, continuously spanning several glacial–interglacial cycles, are restricted to a few studies. For instance, speleothem records from North and South America support orbital parameters as the predominant driver of glacial terminations, although they are limited to the two most recent cycles (Cruz et al., 2005, 2009; Moseley et al., 2016). Another notable example is the case of Chinese speleothems that provided a great paleoclimatic assembled record of the Asian monsoon lasting 640 kyr and encompassing various deglaciations (Yuan et al., 2004; Cheng et al., 2006, 2009, 2016). They even reported first insights into the existence of the extra glacial termination TIII.a, which reproduces patterns of events equivalent to other glacial terminations despite being amid MIS 7 (Cheng et al., 2009). Superimposed on a strong precessional $\delta^{18}O$ signal forced by regional insolation and sea surface temperature gradients, these precisely dated speleothem records from Sanbao cave in China show positive $\delta^{18}O$ anomalies interpreted to reflect changes in the position and timing of monsoon rainfall coincident with the weakening of the AMOC in the North Atlantic (Wang, 2001; Cheng et al., 2009; Cai et al., 2015; Barker and Knorr, 2021; Jian et al., 2022). If AMOC weakening is linked to glacial meltwater release in the North Atlantic, these records may, therefore, provide indirect indicators of the chronology of glacial terminations. However, the distinctive freshening signature of the glacial terminations and therefore the specific time sequence of its events cannot be recorded in these speleothems located far from the North Atlantic water sources. Hence, well-constrained speleothem records capable of recording the North Atlantic deglacial features through its isotopic signature would be advantageous to establish independent chronology on North Atlantic marine sequences and clarify the forcings of deglaciations. In this respect, the first high-resolution speleothem records suc-

cessfully used to tune marine records were collected in the NW Iberia peninsula and documented rapid North Atlantic ice sheet melting spanning the two ultimate glacial terminations (TI and II) at millennial–centennial timescales (Stoll et al., 2022).

Regarding the Mediterranean region, available speleothem records that can be potentially used for marine alignments are mostly restricted to the two most recent deglaciations (e.g., Bar-Matthews et al., 1999, 2000, 2003; Drysdale et al., 2009; Tzedakis et al., 2018). In the western Mediterranean basin, only the Ejulve speleothem record from the eastern Iberian Peninsula detected millennial-scale events related to AMOC slowdowns at TIII (Pérez-Mejías et al., 2017), while speleothems spanning TIV and TV remain elusive in the Mediterranean context (Kaushal et al., 2024). This study presents two new speleothem records from the Balearic islands located in the western Mediterranean region (Fig. 1). The VALL 2 speleothem was recovered from Mallorca and encompassed the TV, whereas the RAT speleothem, recovered from Menorca, encompassed two glacial–interglacial cycles with the chronologies for the glacial terminations TIV, TIII, and TIII.a being well-constrained. Hence, the RAT speleothem offers a unique continuous record not provided by any existing stalagmite archive within this region. A geochemical multiproxy approach has been applied in these two speleothems to investigate climate variability, with a special focus on their glacial terminations. The studied deglaciations present different intensities and durations and open an opportunity to investigate the relationship between orbital parameters and paleoclimatic records. We apply the RAT chronology to newly acquired planktic isotope measurements from the Ocean Drilling Program (ODP) 977 site in the Alboran Sea, highlighting the potential of this speleothem record as a referential base for marine chronologies. This approach aims to avoid the circularity of trying to understand the drivers and thresholds of climate variability using marine chronologies dependent on orbital tuning.

2 Material and methods

2.1 Cave settings and regional hydroclimate

The speleothem called Ratpenat (RAT) was collected from inside Murada cave in Menorca (Fig. 1). The Murada cave is located close to the coast and at a low altitude, 80 m a.s.l., in the southwest area of the island (39°57′58″ N, 3°57′53″ E). This cave is the largest in the Barranc d'Algendar, which is a canyon formed by a ravine cutting Miocene calcarenite rocks, which is where a karst was developed. Nowadays, this cave represents a fossil level of the karst drainage conduit. The RAT speleothem was found broken in two pieces, which were matched in the cave. The VALL 2 speleothem grew inside the d'Es Pas de Vallgornera cave, which is located in the southern part of Mallorca (39°22′00″ N, 2°52′25″ E) (Fig. 1). This cave was also developed in upper Miocene rocks and consists of more than 67 km of conduits and chambers, some of them flooded. Sea level reconstruction by means of overgrowths on speleothems has been previously studied in this cave (Dorale et al., 2010).

According to the Köppen climate classification, the Balearic islands present a temperate climate (Csa) with seasonal rainfall, intense storms in autumn, and dry/hot summers that cause the lack of permanent watercourses. The two main origins of the precipitation on the western Mediterranean Sea are the Mediterranean Sea itself and the tropical–subtropical North Atlantic corridor via the dominant eastward atmospheric circulation, leading storm tracks reaching the Mediterranean (Gimeno et al., 2010; Nieto et al., 2010; Krklec and Domínguez-Villar, 2014; Dumitru et al., 2017; Moreno et al., 2021). However, the major source of moisture for precipitation in the Mediterranean surrounding land area has been identified as the basin itself (Schicker et al., 2010). Particularly in the location of the Balearic islands, the moisture is provided by evaporation over the Mediterranean because of the occurrence of back-door cold fronts related to easterly advection leading to heavy precipitation in autumn (Millán et al., 2005; Moreno et al., 2021). The Mediterranean region has important climate contrasts among different nearby areas because it is a transitional zone between subtropical and midlatitude temperate regimens (Lionello, 2012). While the northern part of the Mediterranean region is strongly linked to midlatitude variability, mostly characterized by the North Atlantic Oscillation, the southern and eastern parts are exposed indirectly to the influences of the Intertropical Convergence Zone (ITCZ) dynamics.

2.2 Geochemical analyses of speleothems

2.2.1 Geochronology

In order to determine the absolute ages, both speleothems were longitudinally cut with a saw, taking into account the morphology and the growth axis. The sampling for measuring uranium and thorium isotopes was designed considering the layering to detect possible hiatuses and changes in growth rates. RAT is a 50 cm long speleothem broken at the top; a 2 cm calcite piece was missing when the sample was found in the cave. It does not reveal important changes in the orientation of the growth axis but presents a prominent orange–brown layer at 14 cm from the tip and white layers at 19 and 33 cm (Fig. 2). The VALL 2 speleothem is a wide and dark brown speleothem that is 22 cm long (Fig. A1 in the Appendix). The color at the bottom of the speleothem is light brown, with a porous texture that, towards the top, becomes darker and less porous. The axis presents several changes in the growth direction and possible discontinuities are characterized by light layers. After the last main discontinuity, the speleothem presents two independent growths. The axis selected to accomplish the analyses follows the most developed axis of the last two growths.

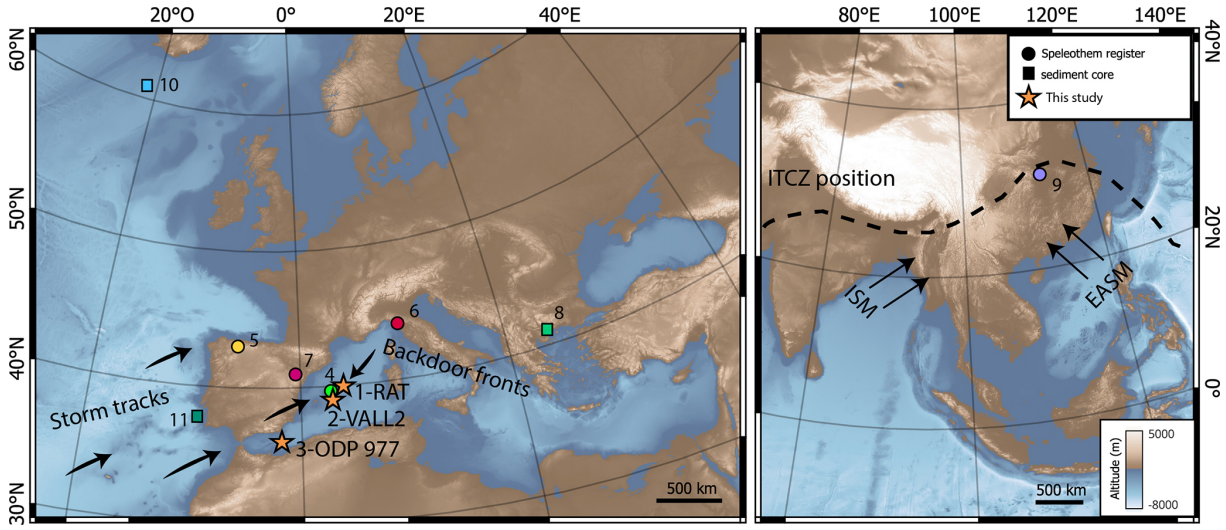

Figure 1. Map showing the location of this study records. (1) Murada cave, on Menorca, where the RAT speleothem was recovered. (2) Vallgornera cave on Mallorca, where the VALL 2 speleothem was recovered. (3) The marine sediment ODP 977 site. Other sites discussed in the text are also shown as follows. (4) Campanet cave on Mallorca (Dumitru et al., 2018). (5) North Iberian Speleothem Archive (NISA) and Garth speleothem records from north Iberia caves (Stoll et al., 2015, 2022). (6) Corchia cave (Drysdale et al., 2004; Tzedakis et al., 2018). (7) Ejulve cave (Pérez-Mejías et al., 2017). (8) The Tenaghi Philippon arboreal pollen record (Tzedakis et al., 2006). (9) Sanbao speleothem record (Cheng et al., 2009, 2016). (10) The ODP 983 site (Barker et al., 2015, 2019; Barker and Knorr, 2021). (11) The MD01-2444 marine core (Tzedakis et al., 2018; Hodell et al., 2023). The map shows the dominant atmospheric circulation that brings moisture to the Balearic islands (via Mediterranean back-door cold fronts and winter storm tracks). Moisture in Asia is related to the dynamics of the East Asian summer monsoon (EASM) and the Indian summer monsoon (ISM), which depends on the Intertropical Convergence Zone (ITCZ). The map shows the modern average position of the ITCZ in summer.

Samples for U / Th analyses were milled with a 2 mm diameter tungsten carbide micro-drill under a laminar airflow cabinet to prevent contamination. About 100–200 mg of carbonate powder was obtained for each sample. The chemical procedure for isolating uranium and thorium elements was performed in the ultra-clean laboratory at the University of Minnesota and Xi'an Jiaotong University, applying the methodology previously described by Shen et al. (2002) and Cheng et al. (2009) (Appendix A). Several blanks were performed routinely for each laboratory sampling set. The radiogenic isotopes of U and Th were analyzed using a parallel ion-counting multi-collector inductively coupled plasma mass spectrometry (MC-ICP-MS) with a Finnigan Neptune model at both universities. The results of these analyses and the absolute dates are detailed in Table A1. The speleothem depth–age models were performed with R software and the StalAge package (Scholz and Hoffmann, 2011), using 39 radiometric dates for RAT and 12 for VALL 2. The RAT speleothem provided a consistent chronology, with a few single dates exceeding the final modeled dating uncertainty. It presents a remarkably precise age model with absolute uncertainties being even smaller in the youngest part of the speleothem (Fig. 2). In contrast, the dates obtained from the VALL 2 speleothem are approaching the limits of the U-series dating technique, thereby resulting in significant uncertainties that are even larger in the oldest section of the speleothem, where the growth rate is higher (Fig. A1). The growth rates range between 0.02–1.2 cm kyr^{-1} for VALL 2 and 0.07–1.7 cm kyr^{-1} for RAT.

2.2.2 Geochemical measurements

Stable isotopes and trace elements have been measured on aliquots of the same powder sample in both speleothems. The δ^{18}O, δ^{13}C, and Mg / Ca ratios have been compared in detail to evaluate their paleoclimatic signals. Samples were drilled using a 0.5 mm diameter tungsten carbide dental burr along the speleothem growth axis. The sample resolution is 2 mm in VALL 2 and 2.5 mm in RAT. However, samples are spaced every 0.5 mm during glacial terminations in the RAT speleothem to increase the temporal resolution due to low growth rates, ensuring that events are captured by more than one measurement.

The δ^{18}O and δ^{13}C measurements were performed with 50 µg of carbonate powder and were accomplished on a Finnigan MAT252 mass spectrometer (isotope ratio mass spectrometer, IRMS) at the Scientific and Technological Centres at the University of Barcelona (CCiTUB). This mass spectrometer is coupled in a single acid bath CarboKiel-III carbonate preparation device to convert solid carbonate samples into simple gas (CO_2) before entering into the ion source of the IRMS. Analytical uncertainties were obtained utilizing two in-house carbonate standards that were calibrated

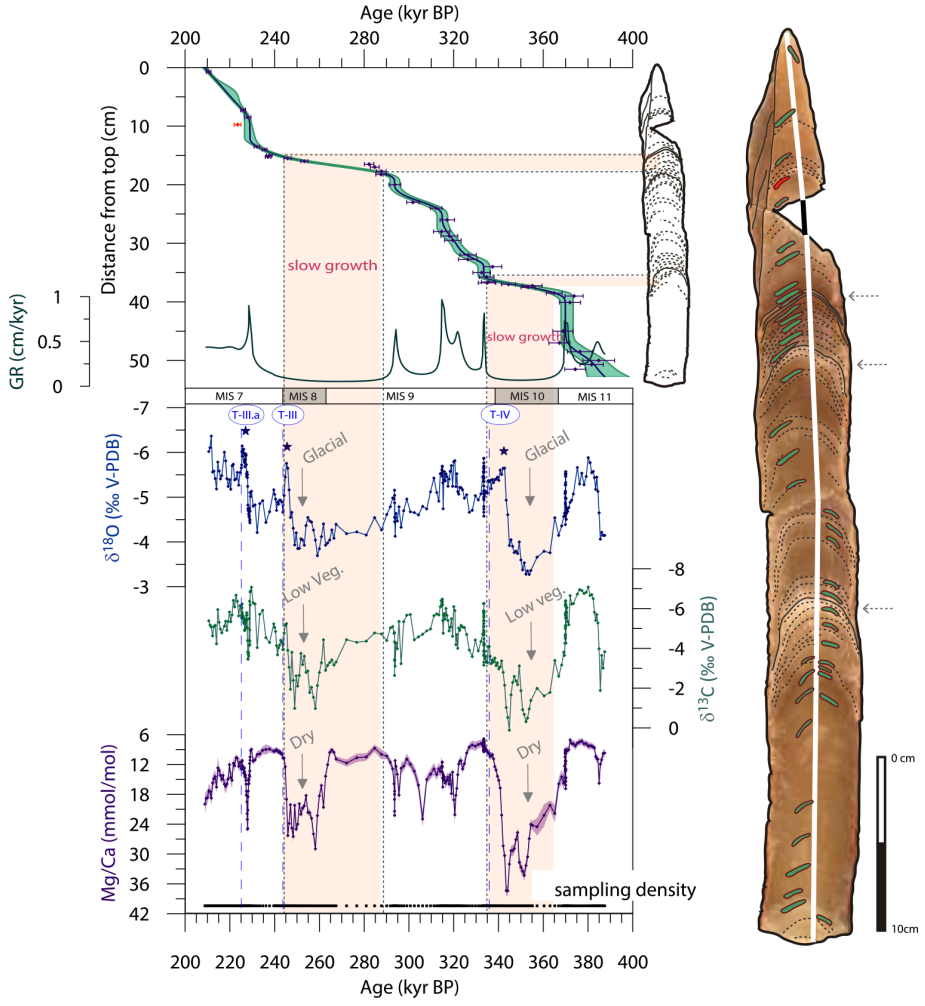

Figure 2. On the right, there is an image of the RAT speleothem showing the positions of the radiometric dates sampled for creating the age model (green) and the reversal not used (red). The growth axis path used for the geochemical analyses is highlighted with a white line. At the top left, the age model acquired by StalAge (dark blue line) and the original U / Th dates for the RAT speleothem (dark blue dots) are plotted with the associated errors (error bars and green area). RAT growth rates are shown in dark green. In the lower panel, the results of $\delta^{18}O$, $\delta^{13}C$, and Mg / Ca ratios are accompanied by uncertainties represented as a shaded area. Note that the three parameters are plotted with a reversed axis. The stars highlight negative $\delta^{18}O$ anomalies mentioned in the main text. The pink bars highlight slow growth rate periods, and the dashed grey line points to major color changes in the speleothem layers, also noted as dashed grey arrows in the image.

to NBS19 international standard (Coplen, 1996). The uncertainties were ≤ 0.04 ‰ Vienna Pee Dee Belemnite (VPDB) for $\delta^{13}C$ and 0.08 ‰ VPDB for $\delta^{18}O$.

Around 3 mg of carbonate powder was used to measure Ca, Mg, and other trace elements such as Ba and Sr to obtain element / calcium ratios. The powder was directly dissolved with 2 mL of ultrapure 2 % HNO_3 (with Rh and Sc as internal standards) and centrifuged to prevent possible lithic particles or impurities in the solution before the analyses. These samples were analyzed employing inductively coupled plasma mass spectrometry (ICP-MS), with an Agilent 7500CE model, at the CCiTUB. Possible contamination was controlled by means of chemistry blank analyses on random days. An in-house high-purity standard solution was measured routinely every four samples to control the accuracy of the measurements. According to the in-house standard analysis, the external reproducibility obtained for the speleothem analyses was 0.86 % (%, 2σ).

2.3 $\delta^{18}O$ Analyses in planktic foraminifera from ODP 977 site

ODP site 977 was retrieved during leg 161 of the Ocean Drilling Program on board the research vessel (R/V) *JOIDES Resolution*. It was located halfway between the Spanish and Algerian coasts, in the eastern sub-basin of the Alboran Sea, at 36°01.92′ N and 1°57.32′ W and at a water depth of 1984 m b.s.l. (meters below sea level; Fig. 1). This study ex-

tends the oxygen isotope data obtained in previous studies of this sediment core (Martrat et al., 2004, 2007; Gonzalez-Mora et al., 2008; Torner et al., 2019; Azibeiro et al., 2021). The ODP 977 age models of all these different studies are mostly based on the original age model from Martrat et al. (2004), which is established on the correlation between its *Globigerina bulloides* $\delta^{18}O$ curve and the SPECMAP stacked curve (Martinson et al., 1987). However, in Torner et al. (2019) some additional tie points were used to align the TII with other Mediterranean cores radiometrically tuned with speleothems. Azibeiro et al. (2021) adjusted the age model along the TV by aligning its alkenone-based sea surface temperature (SST) record to North Atlantic midlatitude temperature records.

Stable isotopes on planktic foraminifers were performed on handpicked specimens of *G. bulloides*. Shells were crushed between two glass plates to open the chambers and favor the following clay removal. Afterward, samples were cleaned with methanol and sonicated for a few seconds. The supernatant solution was removed with a micropipette, and finally, the samples were dried. The measurements were accomplished by isotope ratio mass spectrometry at the CCiTUB using the same analytical method that was previously explained for speleothems analyses.

3 Results and discussion

3.1 The climate signal in the speleothems

Mg / Ca ratios and stable isotopes in both speleothems reveal climate variability in the western Mediterranean region. According to the obtained depth–age models, VALL 2 spans from 530 to 345 ka (MIS 13–MIS 11), encompassing the glacial termination V, while RAT spans from 387 to 209 ka (MIS 11–MIS 7), continuously covering an exceptionally long time interval (178 kyr) that includes three glacial terminations (TIV, TIII, and TIII.a). Glacial conditions are characterized by slower growth rates and high $\delta^{18}O$, $\delta^{13}C$, and Mg / Ca, while the warm MISs feature low isotopes and Mg / Ca ratios (Fig. 2 and Appendix A1). The RAT record presents an overall variation of 3.2 ‰, 6.3 ‰ and 24.6 mmol mol^{-1} for $\delta^{18}O$, $\delta^{13}C$, and Mg / Ca, respectively. And the overall variation is 3.4 ‰, 3.8 ‰, and 15.7 mmol mol^{-1} in the VALL 2 speleothem. Given the insufficient robustness of the VALL 2 age model for the precise evaluation of climatic events, the discussion is primarily focused on the RAT results.

The Mg / Ca ratio in speleothems is sensitive to variations in the precipitation/evaporation balance, reflecting changes in the amount of water infiltrating into the karst system. Frequently, arid conditions, characterized by reduced water infiltration, may increase the groundwater residence time in the karst and even reduce drip rates in the caves (Fairchild et al., 2000). This scenario provides an opportunity to enhance the degassing of groundwater, thereby facilitating carbonate precipitation prior to the arrival of drip water at the surface of the speleothem. This process, known as prior calcite precipitation (PCP), can also be favored by reductions in the partial pressure of CO_2 (pCO_2) within the cave atmosphere. Ventilation typically reduces the CO_2 levels in the cave and occurs when external cooling provokes an exchange of air between the internal and external atmosphere. This mechanism typically occurs on a seasonal scale, and, presuming that the cave structure has remained constant over time, this influence would persist throughout glacial and interglacial periods, exerting a minor impact on the millennial timescale. Moreover, cold and arid conditions cause a decline in vegetation activity, leading to lower respiration rates and diminished CO_2 liberation. Briefly, processes that reduce pCO_2 in the karstic system support PCP. This PCP can preferentially remove Ca from the drip waters, consequently elevating the trace element / Ca ratio of all incompatible elements in the drip waters, such as Mg / Ca, Sr / Ca, and Ba / Ca. When the partitioning coefficients of Mg, Sr, and Ba in stalagmite calcite are relatively stable, the speleothem Mg / Ca, Sr / Ca, and Ba / Ca reflect this drip water PCP signature. The RAT Sr / Ca and Ba / Ca records show similar temporal variations to the Mg / Ca variability (Fig. A2), suggesting that all three elements are dominated by a common process of PCP. The magnitude of change in Mg / Ca is much larger than what would arise due to temperature-driven changes in Mg partitioning, which, in any case, would elevate Mg incorporation during warm interglacials and is in contrast to the observed pattern. PCP can also be enhanced by higher drip water saturation states, even with constant drip rates (Stoll et al., 2012), but the observation of maximum PCP during cold glacial periods characterized by lower soil CO_2 due to diminished microbial activity and vegetation respiration rates and likely lower initial drip water saturation suggests that elevated glacial PCP is caused by slower drip rates and is driven by lower infiltration and lower precipitation–evapotranspiration.

Speleothem $\delta^{13}C$ can also reflect hydroclimate variations. The initial $\delta^{13}C$ of the drip water reflects a mixing signal derived from the carbon isotopic composition signatures of limestone, atmospheric CO_2, and the biogenic soil gas derived from both the microbial activity and the vegetation respiration (Hellstrom et al., 1998). Soil autotrophic and heterotrophic respiration typically have lower $\delta^{13}C$ values. Hence, cold and dry conditions can depress soil respiration rates and contribute to an increase in the $\delta^{13}C$. Likewise, the concentration of atmospheric CO_2 (with a higher $\delta^{13}C$ signal) would be proportionally higher than the relatively low biogenic carbon signature in the soil gas, elevating the $\delta^{13}C$ values even more. It is for that reason that many midlatitude speleothem studies interpret high $\delta^{13}C$ as reflecting reduced soil/vegetation activity (Genty et al., 2013; Moreno et al., 2010; Bartolomé et al., 2015; Pérez-Mejías et al., 2017). Additionally, slowed drip rates during dry periods may contribute to greater PCP, which also causes drip water to evolve

to higher $\delta^{13}C$ due to the gradual loss of the light isotope. Thus, via these two processes (initial drip water changes and PCP), dry conditions may contribute to higher speleothem $\delta^{13}C$. In the RAT record, while cold temperatures likely depressed soil respiration during glacials and contributed to the high $\delta^{13}C$, the general co-variation between Mg / Ca and $\delta^{13}C$ suggests that the high glacial $\delta^{13}C$ also reflects drier conditions contributing to low soil CO_2 and slower drip rates favoring more extensive PCP. In another speleothem record from Mallorca, high $\delta^{13}C$ was similarly interpreted to reflect low biogenic CO_2 productivity in soil and/or a short water residence time, reflecting dry conditions (Dumitru et al., 2018). The RAT $\delta^{13}C$ signal shows a smoothed signal with respect to the Mg / Ca during glacial terminations, suggesting a slower response of the vegetation compared with precipitation rises (Fig. 2). MIS 11, MIS 9, and MIS 7 were characterized by enhanced precipitation conditions that led to higher soil respiration activity under more extensive vegetation.

The $\delta^{18}O$ RAT record is marked by higher $\delta^{18}O$ during glacials and lower $\delta^{18}O$ during interglacials (Fig. 2). On a global scale, the retreat of the large continental Northern Hemisphere ice volume and release of meltwater lowers the $\delta^{18}O_{sw}$ in the surface ocean. This lower $\delta^{18}O_{sw}$ causes a corresponding decrease in the $\delta^{18}O$ of rainfall and the drip waters from which the speleothem is formed, lowering the speleothem $\delta^{18}O$. Over the most recent glacial cycles, the North Atlantic experiences a greater amplitude change in $\delta^{18}O_{sw}$ than the globally averaged surface ocean (Waelbroeck et al., 2014). In some regions, major changes in atmospheric circulation patterns cause additional larger changes in rainfall $\delta^{18}O$ which significantly exceed the effect of the surface $\delta^{18}O_{sw}$. In coastal regions of the North Atlantic, the change in the surface ocean isotopic composition is a dominant component of speleothem $\delta^{18}O$ variations over glacial terminations (Stoll et al., 2022). A comparison of independently dated marine $\delta^{18}O_{sw}$ with speleothem $\delta^{18}O$ records from NW Iberia showed that the speleothem $\delta^{18}O$ matched the timing and amplitude of the $\delta^{18}O_{sw}$ shift in the eastern North Atlantic during termination I (Stoll et al., 2022). Furthermore, several studies demonstrate that the North Atlantic $\delta^{18}O_{sw}$ signal, changed by those freshwater inputs, was transferred into the Mediterranean Sea (Cacho et al., 1999; Sierro et al., 2005; Jiménez-Amat and Zahn, 2015; Marino et al., 2015). Over termination I, the North Atlantic $\delta^{18}O_{sw}$ decreased rapidly at around 16 ka and between 12 and 10 ka, and these two shifts are also recorded in the Alboran Sea, as well as around Menorca (Fig. A3). Consequently, we propose that the RAT $\delta^{18}O$ records the change in $\delta^{18}O_{sw}$ in the moisture source area for the precipitation, encompassing global changes in the $\delta^{18}O_{sw}$ at a large scale and superimposing the freshening signal transmitted to the Mediterranean Sea during deglaciations. This is also supported by the evaluation of the isotopic composition of rainfall waters and cave drip waters in Mallorca, which points to the western Mediterranean as the dominant source for moisture uptake in coastal caves (Dumitru et al., 2017). The cave location of this study, close to the coast and at a low altitude above sea level, should minimize distillation processes, and therefore, RAT $\delta^{18}O$ captures the signal of the moisture source, which is surface water mostly from the western Mediterranean.

3.2 Mediterranean precipitation modulated by precession

The RAT Mg / Ca record shows a clear precession pattern. Low Mg / Ca, indicating enhanced precipitation, coincides with precession minima, which are times of the high Northern Hemisphere summer insolation (NHSI) (Fig. 3; pink bars), and vice versa for drier periods. The most humid periods are recorded during the strong precession minima of the marine isotopic sub-stages of MIS 9e, MIS 9a, and MIS 7e. MIS 11a shows similar humidity despite a moderate precessional minimum. The low resolution of the Mg / Ca record during the MIS 9a precludes us from evaluating its duration and structure. In the better-resolved interglacial acmes of MIS 9e and MIS 7e, we estimate a duration of $\sim$ 10 kyr. These orbitally paced changes in Mediterranean precipitation are explained because minima precession led to higher seasonality (high NHSI – low Northern Hemisphere winter insolation, NHWI), which intensified wintertime storm tracks and increased the Mediterranean precipitation. Additionally, higher air–sea temperature gradients enhanced evaporation from the Mediterranean basin itself, leading to greater local convective precipitation (Kutzbach et al., 2014; Wagner et al., 2019; García-Alix et al., 2021).

This new and uninterrupted record covers enough time to confirm the precession imprint for the first time in a Mediterranean speleothem. Other European speleothems have also recorded enhanced precipitation during precession minima of the studied interglacials; however, they provide shorter records. The iconic $\delta^{18}O$ record of the Antro del Corchia cave, from Italy, shows periods of greater humidity that are in line with those recorded in RAT during the MIS 9 (Drysdale et al., 2004; Tzedakis et al., 2018). However, higher U / Th date uncertainties could account for some chronological discrepancies (Fig. 3). The increment in moisture availability in western Italy was attributed to regional warm SST that led to enhanced evaporation (Drysdale et al., 2004). Carbon isotope records from other European speleothems are more complex to interpret without accompanying trace elements, but the trends are consistent with warmth and/or greater humidity during MIS 7e. The $\delta^{13}C$ speleothem record from the Ejulve cave, in the northeastern Iberian Peninsula, shows lower values during MIS 7e (Fig. 3) and is interpreted as a proxy for vegetation productivity (Pérez-Mejías et al., 2017). Considering that the typical dating error in the RAT record along the MIS 7e averages $\sim$ 1.2 kyr and that the Ejulve error record averages $\sim$ 2 kyr, both records strengthen the enhanced humidity along this period. Other speleothem records

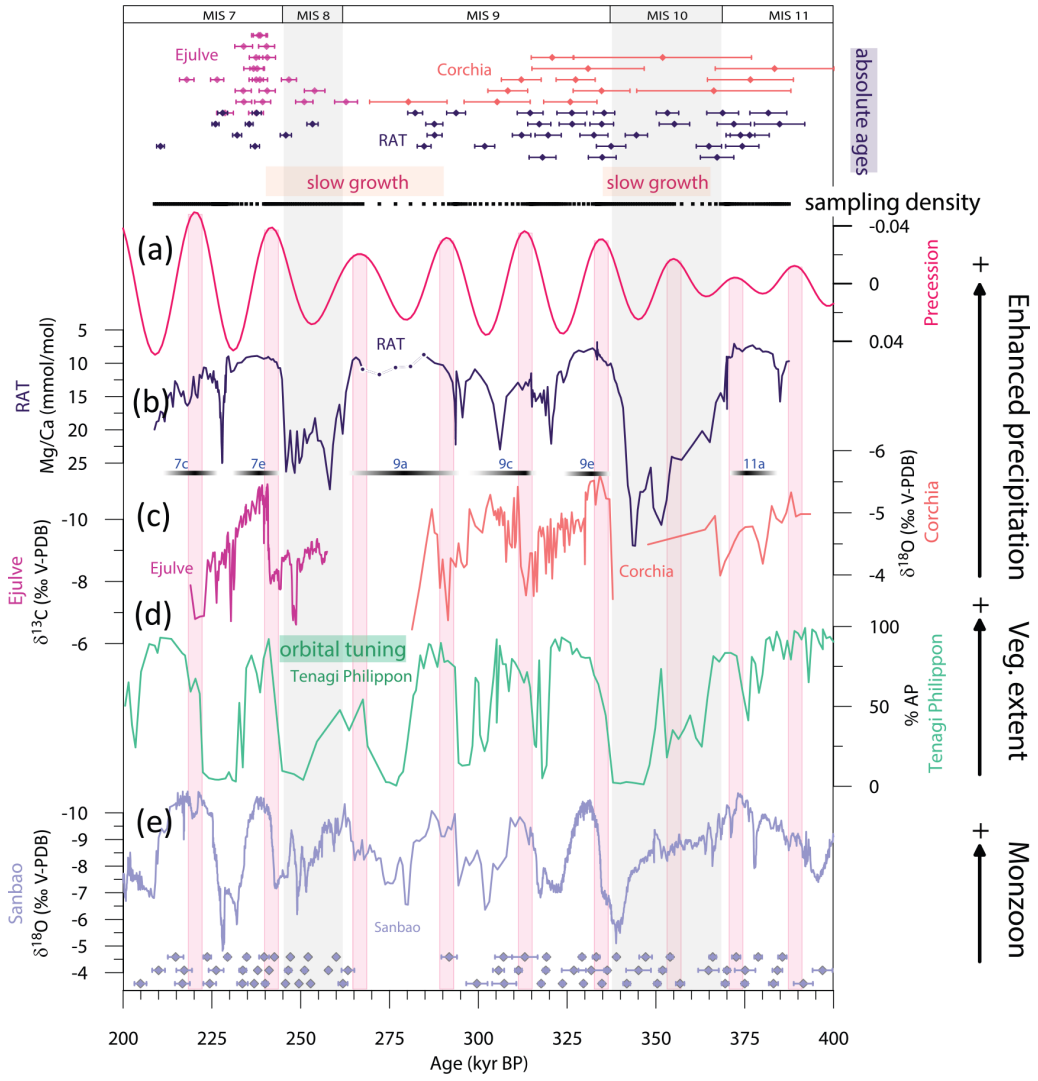

Figure 3. The RAT speleothem U / Th ages with the 2σ error bars are found at the top of the figure, together with the speleothem dates from the Ejulve and Corchia caves. **(a)** Precession curve with vertical pink bars highlighting minima precession (Laskar et al., 2004). **(b)** RAT Mg / Ca record with periods of enhanced precipitation marked with horizontal black lines which correspond to the interglacial/interstadial marine isotopic stages (MISs). **(c)** The $\delta^{18}O_{speleo}$ Corchia record (Drysdale et al., 2004; Tzedakis et al., 2018) and the $\delta^{13}C_{speleo}$ record from the Ejulve cave (Pérez-Mejías et al., 2017). **(d)** The Tenaghi Philippon arboreal pollen record from Greece (Tzedakis et al., 2006). **(e)** The $\delta^{18}O_{speleo}$ record from the Sanbao cave in China with the U / Th ages and 2σ error bars (Cheng et al., 2016).

from the Austrian Alps (~ 0.3 kyr average errors) and Sardinia (~ 1.5 kyr average errors) also reflect warming or more humid conditions along the MIS 7e responding to changes in the North Atlantic realm (Spötl et al., 2008; Columbu et al., 2019; Wendt et al., 2021).

Similarly, long-term pollen records of the Mediterranean region show expansions of the arboreal vegetation coincident with precession minima because of warmer climate and greater water availability (Sánchez-Goñi et al., 2008; Tzedakis et al., 2006, 2009; Wagner et al., 2019). In particular, the arboreal pollen percentages in the Tenaghi Philippon pollen record from Greece, in the eastern Mediterranean region, show an extraordinary resemblance with the precipitation variability recorded in the RAT Mg / Ca, where high arboreal pollen percentages are in line with enhanced precipitation (Fig. 3) (Tzedakis, 2003; Tzedakis et al., 2006). However, certain time discrepancies can be observed mostly during the end of the glacial MIS 10 and for the TIV and TIII.a. The Tenaghi Philippon age model relies on orbital tuning, assuming a constant lag of 1000 years in the orbital alignment, a circumstance that may account for certain discrepancies with the absolutely dated speleothem record. Aside from the age biases during deglaciations, both records exhibit proxy fluctuations associated with glacial/interglacial cycles,

as well as stadial/interstadial structures with a strong precession signal.

Precession has a major effect on the Mediterranean Sea due to its ability to disrupt the evaporation-precipitation balance of the sea basin. This influence has been documented through several proxy records that demonstrate modifications in oceanographic and sedimentary processes. For instance, marine sediment records close to the Strait of Gibraltar recorded changes in the Mediterranean Outflow Water (MOW) strength, mainly driven by precession-controlled fluctuations in the Mediterranean hydrologic budget (Nichols et al., 2020; Sierro et al., 2020), and marine sediments from the Balearic Sea documented carbonate cyclicities due to the control of the western Mediterranean cyclogenetic mechanisms (Ochoa et al., 2018). The precession control on the African monsoon is well known, which indirectly also affected the eastern Mediterranean water properties through river runoff along the north African coast, drastically changing the $\delta^{18}O_{sw}$ composition and allowing sapropel formations (Rohling et al., 2014; Grant et al., 2016). Several studies highlight that the timing of enhanced summer monsoon corresponds with maximum Mediterranean autumn/winter storm track precipitation (Kutzbach et al., 2014; Toucanne et al., 2015; Wagner et al., 2019). The Mg / Ca RAT record also reveals this concordance, where western Mediterranean enhanced precipitation, during interglacial/interstadial periods of precession minima, is consistently in line with higher summer monsoon intensities according to the Chinese speleothem records from Sanbao cave (Fig. 3) (Cheng et al., 2016).

3.3 Onset of glacial terminations

The newly obtained RAT records provide new constraints on the absolute age for glacial terminations TIV, TIII, and TIII.a based on the identification of meltwater release reflected in negative $\delta^{18}O$ excursions (Fig. 4a). Accordingly, the onset of TIV shows a first $\delta^{18}O$ depletion at 351 ± 5 ka, followed by a larger depletion at 343 ± 3 ka, which likely reflects the maximum rate of ice melting. This is consistent with a study based on volcanic interbed deposits of near-coastal aggradational successions in Italy (Fig. 4a; horizontal purple bars), which provided independent ages for sea level rise by means of ^{40}Ar / ^{39}Ar absolute dating (Marra et al., 2016, 2019). The onset of the TIII in the RAT speleothem is also in concordance with the sea level rise observed in Italy, and the principal $\delta^{18}O$ negative anomaly occurred at 245 ± 2 ka. This anomaly is comparable in magnitude to the TIV freshening. The TIII.a deglaciation is marked by the negative $\delta^{18}O$ anomaly centered at 227 ± 1 ka (Fig. 4). This characteristic $\delta^{18}O$ feature of deglaciations is also recognized in the Mallorca speleothem (VALL 2) along the TV, although the high age uncertainties associated with the chronological limit of the U–Th technique preclude a precise date for the onset of this termination (Fig. A1).

The peaks of maximum freshening for the three studied glacial terminations in RAT occurred during the falling precession index and are, therefore, consistent with the beginning of the summer insolation increases (Fig. 4b). In contrast, the obliquity phase is very variable among the three terminations. The TIV and TIII.a occurred during the obliquity increase, while this parameter was decreased through TIII. Hence, falling precession is the common orbital feature along the studied terminations, supporting the idea that precession appears more important than obliquity in predicting the onset of Late Pleistocene glacial terminations (Hobart et al., 2023). Tzedakis et al. (2017) proposed that the energy needed to force the glacial terminations also depends on the length and the intensity of the previous glacial period. The evaluation of the glacial conditions also reveals differences among the three studied terminations. Robust glacial conditions properly preconditioned the continental ice sheet volume before the TIV deglaciation. Lower precession amplitude, together with minimum obliquity through the full glacial conditions of the MIS 10, led to less caloric summer insolation before the TIV onset, strengthening the glacial maximum conditions. The caloric summer insolation is controlled by the combination of precession and obliquity and represents the amount of energy integrated over the caloric summer half of the year, certainly playing a causal role in the achievement of interglacial acmes (Milankovitch, 1941; Tzedakis et al., 2006). But it should also influence glacial attributes. MIS 10 culminated with a maximum in the ice sheet extent according to the benthic $\delta^{18}O$ record from the LR04 stack (Lisiecki and Raymo, 2005), but this was also observable in the more extreme positive glacial $\delta^{18}O$ in the $\delta^{18}O$ RAT record. Furthermore, IRD was released continuously in the North Atlantic at the end of MIS 10, highlighting freshwater inputs (Fig. 4c) (Barker et al., 2015, 2019; Barker and Knorr, 2021). These intense pre-deglacial conditions facilitated the early freshening phase at the onset of TIV and may have reinforced the duration of the subsequent pronounced freshening and the relaxation time observed in the $\delta^{18}O$ RAT record. The maximum glacial conditions with noticeable IRD release did not present such a prominent ice volume maximum at the end of the MIS 8 in the benthic $\delta^{18}O$ or in the RAT records. This glacial situation favored the shorter and less noticeable freshening of the TIII (Fig. 4c). The $\delta^{18}O$ RAT shows a similar freshening structure between TIII and TIII.a, despite TIII.a being an exceptional deglaciation because it does not proceed from full glacial conditions. Short and cold stadial conditions, with less IRD release and accumulated ice volume, allowed a strong response of the ice sheet dynamics to the insolation rise; this was probably due to the pronounced orbital changes through this deglaciation. Interestingly, the meltwater release of TIII.a culminated significantly before the summer caloric insolation maxima, reinforcing the exceptional character of this extra termination (Fig. 4c), while TIV and TIII are closer to their respective summer caloric insolation maxima. The extent of the studied

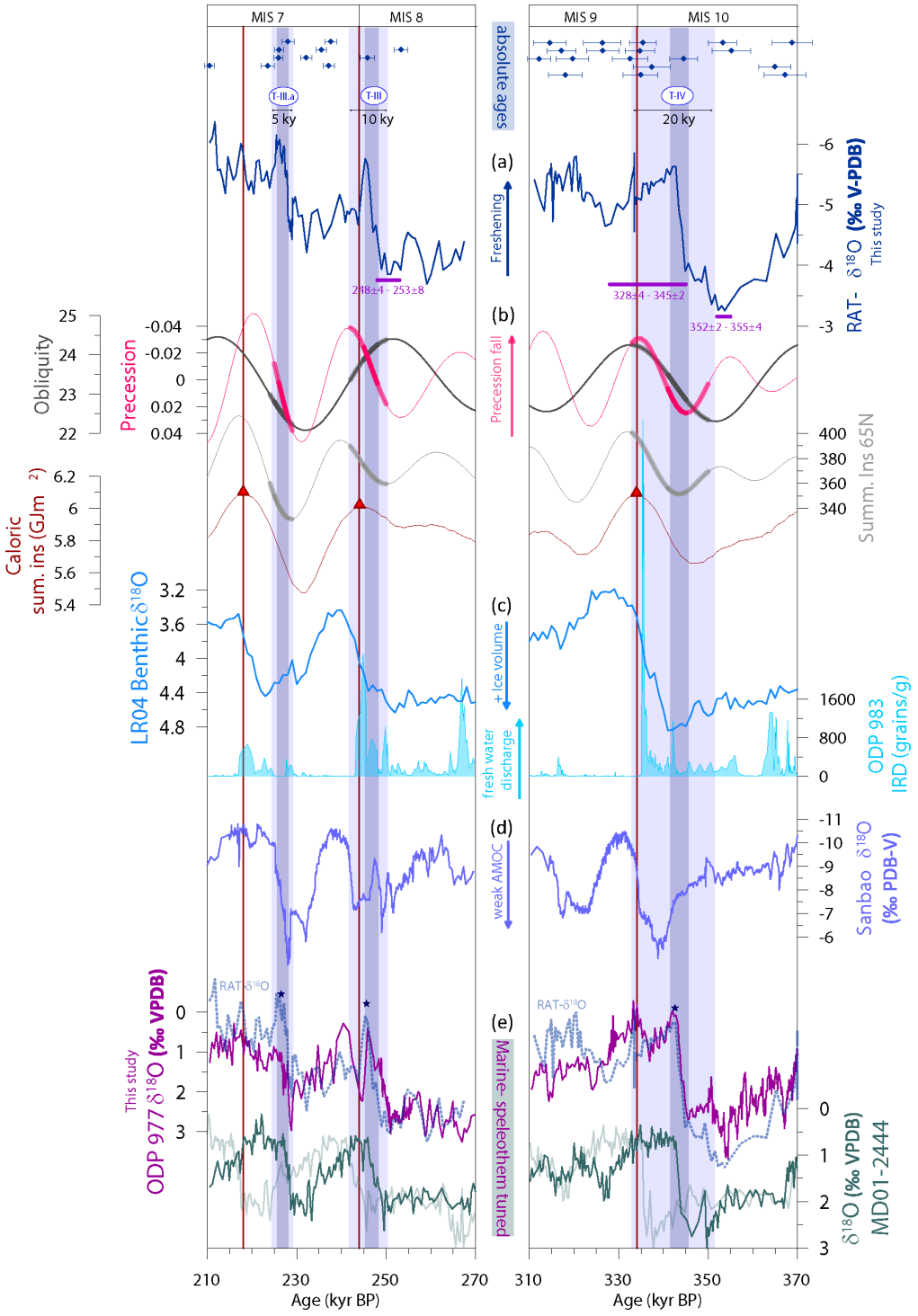

Figure 4. Comparison between glacial termination TIV (right panel) and glacial terminations TIII and TIII.a (left panel). On the top, the RAT U / Th ages with the 2σ error bars. The vertical blue bars highlight the duration of glacial terminations according to the negative $\delta^{18}O$ structures of the RAT record, while the internal and thinner dark blue bars emphasize the maximum rate of freshening discussed in the main text. **(a)** The $\delta^{18}O_{speleo}$ record from RAT speleothem. The horizontal purple lines denote periods of sea level rise according to Marra et al. (2016, 2019). **(b)** Orbital parameters (Laskar et al., 2004) and the caloric summer insolation curve with maximums are highlighted with red triangles (Tzedakis et al., 2006). **(c)** The LR04 stack of $\delta^{18}O$ benthic foraminifera (Lisiecki and Raymo, 2005) and the North Atlantic IRD record of the ODP 983 site (Barker et al., 2015, 2019; Barker and Knorr, 2021). **(d)** The $\delta^{18}O_{speleo}$ record of the Sanbao cave in China (Cheng et al., 2012, 2016). **(e)** $\delta^{18}O_{planktic}$ record from both the ODP 977 site and the MD01-2444 sediment core plotted using the speleo-tuned marine chronologies. The original chronology of the MD01-2444 core is in light green (Hodell et al., 2013).

freshening is in line with AMOC weakening, according to the Chinese Sanbao speleothems (Fig. 4d).

A comparison among the last five glacial terminations is presented in Fig. 5. The studied terminations (TIV, TIII, and TIII.a) are directly compared with terminations TII and TI documented in $\delta^{18}O$ records of Cantabrian speleothems from the north Iberia Peninsula caves (Stoll et al., 2015, 2022). The TII and TI also occurred in line with the falling precession index. In the right panel, all the records were centered at the first and most prominent $\delta^{18}O$ negative anomaly structure in order to compare their duration. The same exercise was performed with the isotopic measurements to observe the freshening magnitudes. This comparison underlines the fact that TIII and TIII.a were the ones with less freshening magnitude, while TIV was prominent. Unlike the benthic $\delta^{18}O$ records, which feature a freshening and plateau at interglacial values, in the speleothem records the peak freshening marked by the negative $\delta^{18}O$ relaxes back to intermediate values. During TII, the period of the most extreme negative $\delta^{18}O$ in north Iberia speleothems indicates fresher surface ocean $\delta^{18}O_{sw}$, highlighting the concentration of meltwater in the North Atlantic, and the relaxation has been interpreted to reflect the mixing of this meltwater anomaly throughout the global ocean as the rate of meltwater addition slows and the rate of overturning circulation strengthens (Stoll et al., 2022). The RAT record suggests differences in the time required from the deglacial onset until the relaxation of these negative $\delta^{18}O$ anomalies from very rapid (~ 5 kyr) during TIII.a, similar to the TI relaxation before the Bölling–Alleröd event; and intermediate (~ 10 kyr) for TIII, similar to TII; to much slower (~ 20 kyr) for TIV (Fig. 5).

3.4 Implications for marine chronologies

The RAT speleothem provides absolute chronologies for the deglacial time sequences in the western Mediterranean, which can be transferred to marine sequences that have proxies which are also sensitive to deglacial freshening. This is the case of the $\delta^{18}O_{planktic}$ data measured in *G. bulloides* from the ODP 977 site in the Alboran Sea, where their combined use with Mg / Ca-derived temperatures has provided $\delta^{18}O_{sw}$ reconstructions that prove the arrival of North Atlantic freshening associated with the major melting phases of mostly the Fennoscandian ice sheets during TV, TIII.a, TII, and TI (Azibeiro et al., 2021; Gonzalez-Mora et al., 2008; Jiménez-Amat and Zahn, 2015; Torner et al., 2019; Stoll et al., 2022). These studies conducted at the ODP 977 site indicate that the timing and magnitude of the main negative $\delta^{18}O_{sw}$ shift are synchronous with $\delta^{18}O_{planktic}$ changes at glacial terminations, suggesting that the freshwater signal may have a dominant influence on the $\delta^{18}O_{planktic}$ variability (Fig. A4). Moreover, the amplitude between the deglacial anomalies of the $\delta^{18}O_{planktic}$ record in the ODP 977 and the $\delta^{18}O$ RAT records is similar for the three studied terminations. Hence, the new $\delta^{18}O_{planktic}$ data for TIV, TIII, and TIII.a provide an exceptional base to tune the millennial-scale features of the marine record to our dated $\delta^{18}O$ RAT record, achieving an orbitally independent chronology. Therefore, the more negative $\delta^{18}O_{planktic}$ structures have been used to align the chronology with the $\delta^{18}O$ negative anomalies of RAT during the glacial terminations. The resulting ODP 977 age model is shown in Fig. A5, where the tie points used by the alignment can be observed. Freshening due to ice melting is notable in the $\delta^{18}O_{planktic}$ ODP 977 signature, and the resemblance with the $\delta^{18}O$ RAT record is remarkable during glacial terminations (Fig. 4e). This new ODP 977 chronology is further applied to records from the Iberian Atlantic Margin (MD01-2444), which also contains deglacial negative $\delta^{18}O_{planktic}$ anomalies (Fig. 4e) (Tzedakis et al., 2018; Hodell et al., 2013). Several tie points have also been used to tune the MD01-2444 in the base of the most relevant structures (Fig. A5). All the correlations among the tuned records were estimated by linear interpolation using the AnalySeries Software package (Paillard et al., 1996). Particularly, the adjusted TIV exhibits a temporal discrepancy of ~ 7.4 kyr compared to the established chronology, and the mean age uncertainty in the RAT speleothem throughout this termination is less than this difference, which is approximately ± 3.4 kyr. In contrast, the TIII aligns well with previously published chronologies due to a minor time discrepancy, which is approximately ~ 3 kyr and similar to the RAT average age uncertainty of ± 1.5 kyr. In the case of TIII.a, the chronological discrepancy is even more significant, reaching ~ 11 kyr, with average errors in the RAT estimated to be around ± 1 kyr. Hence, this exercise reveals significant time discrepancies, particularly for TIV and TIII.a, and exposes that marine chronologies remain unconstrained – mostly for glacial termination onsets. This study supports the idea that millennial-scale variability could strongly influence climate variation along deglaciations (Barker and Knorr, 2021) and highlights that the distinctive characteristic of each glacial termination should be seriously considered to tune the marine chronologies. In addition, it exposes the power of the RAT speleothem as an excellent example to evaluate the time sequences of TIV and TIII.a and encourages the revision of the marine chronologies to clarify glacial termination dynamics independently of the orbital bond.

4 Conclusions

Geochemical proxies in the speleothem RAT reveal alternating dry glacial conditions and wet interglacial conditions in the western Mediterranean region from MIS 11 to MIS 7. Deglaciations were systematically initiated with major ocean freshening events in the North Atlantic and recorded as negative $\delta^{18}O$ anomalies in the speleothem in parallel with extreme arid conditions in the western Mediterranean region according to the Mg / Ca. This study provides further evidence that falling precession was the major orbital trigger for

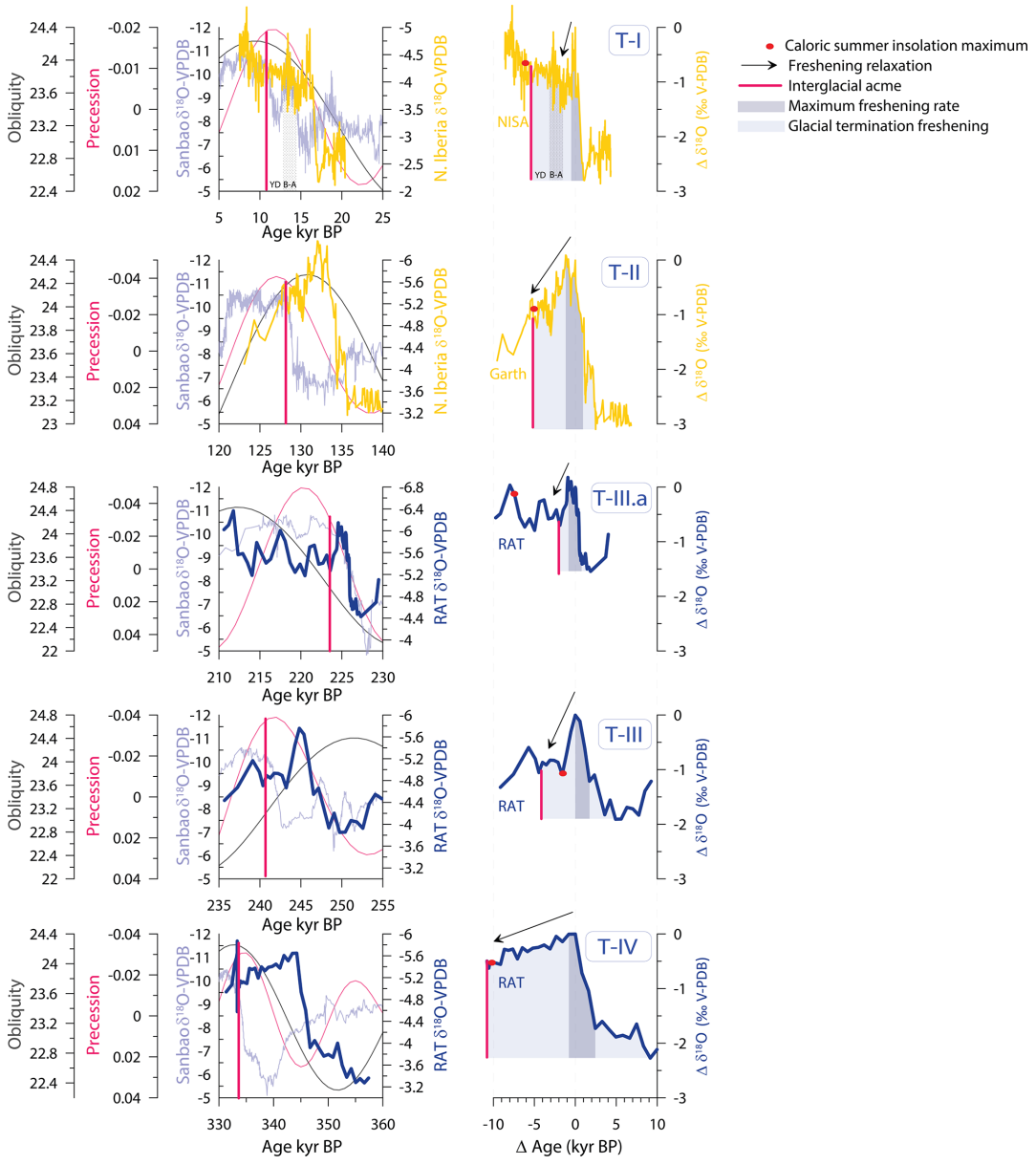

Figure 5. Comparison of the $\delta^{18}O_{speleo}$ records from the RAT speleothem and the north Iberian speleothems (Stoll et al., 2022) along the last five glacial terminations. In the left panel, the speleothem records are plotted against the obliquity and precession parameters (Laskar et al., 2004). The onset of each interglacial acme is highlighted with a vertical pink line according to the Sanbao speleothem record (Cheng et al., 2012, 2016), which considered the recovery of the East Asian summer monsoon intensities as the end of the deglaciation. The right panel shows the duration and the magnitude of the $\delta^{18}O$ freshening structures in Iberia using differential values on the x and y axes. The zero value corresponds to the first and most negative $\delta^{18}O$ value of the main freshening structure of each termination. The black arrow underlines the freshening relaxation of the negative isotopic anomaly after the maximum freshening rate. The maximum summer caloric insolation after each glacial termination is also highlighted with a red circle. It is notable how different the positions of the summer caloric insolation maximum and precession minima are with respect to the freshening structure and the interglacial acme among the compared terminations.

glacial terminations and constrained the deglacial time sequences of each studied glacial termination. Despite the common features, the three deglaciations present differences in terms of magnitude, intensity, and duration. The dissimilarities along the preceding glacial conditions also contributed to these distinctive features. TIV was slower, longer, and more intense than TIII and TIII.a. The RAT record provides an absolute chronology for the intense meltwater release events that initiated the glacial terminations but also for the maximum freshening of each deglaciation, namely TIV onset at 351 ± 5 ka and the maximum freshening peak at 343 ± 3 ka, the TIII onset at 251 ± 3 ka and the maximum

freshening peak at 245 ± 2 ka, and finally the TIII.a onset at 229 ± 2 ka and the maximum freshening peak at 227 ± 1 ka. The newly achieved chronology indicates that revision is needed to the most common marine chronologies, mostly for TIV and TIII.a, which are based on orbital tuning. These discrepancies and the role of millennial-scale variability associated with the onset of glacial terminations suggest that a standard orbital tuning of marine sequences will often not yield a robust chronology. The RAT speleothem provides for the very first time the possibility of validating and improving the accuracy of North Atlantic and western Mediterranean marine chronologies by independent absolute dating.

Appendix A: U / Th laboratory procedure

Speleothem carbonate sample powders were dissolved in 7N HNO_3 and spiked with an in-house solution with known ^{233}U, ^{236}U, and ^{229}Th concentrations. After that, a few drops of concentrated $HClO_4$ were added to attack and remove organic matter. After 1 h of refluxing, the samples were completely dried and re-dissolved in 2N HCl. The U and Th were isolated from Ca and several trace elements by means of an iron co-precipitation. Then, one–two drops of $FeCl_2$ were added, and several NH_4OH drops were added later to induce the Fe precipitation, together with U and Th. Afterward, samples were centrifuged and rinsed with super-clean water three times, while the overlying liquid was removed. In order to separate Fe from U and Th, iron samples were dissolved and loaded in anion exchange resin columns. While Fe was removed with 7N HNO_3, Th was collected with 6N HCl and separated from U, which was recovered ultimately with super-clean water. Each pair of samples was dried and dissolved in a low-concentrated nitric acid and analyzed by means of multi-collector inductively coupled plasma mass spectrometry at the University of Minnesota and Xi'an Jiaotong University. Results and dating errors in the RAT and VALL 2 speleothems are found in Table A1.

https://doi.org/10.5194/cp-21-465-2025

Table A1. U / Th dates from RAT and VALL 2 speleothems.

Speleo	Depth (cm)	^{238}U (ppb)	Error (2σ)	^{232}Th (ppt)	Error (2σ)	^{230}Th / ^{232}Th (atomic $\times 10^{-6}$)	Error (2σ)	δ^{234}U[a] (measur.)	Error (2σ)	^{230}Th / ^{238}U (activity)	Error (2σ)	^{230}Th age (years) (uncor.)	Error (2σ)	^{230}Th age (years)	Error (2σ)	δ^{234}U Initial[b]	Error (2σ)	^{230}Th age (years BP)[c] (corrected)	Error (2σ)
RAT	0.75	186.0	±0.2	1697	±34	3951	±79	1249.1	±2.5	2.1858	±0.0039	210 673	±1087	210 591	±1088	2263	±8	210 525	±1088
RAT	7.25	125.6	±0.1	1179	±24	3947	±79	1246.2	±2.2	2.2458	±0.0033	226 066	±1054	225 984	±1055	2358	±8	225 918	±1055
RAT	7.25	177.3	±0.1	106	±2	62119	±1434	1257.5	±1.9	2.2584	±0.0033	226 101	±993	226 095	±993	2380	±8	226 024	±993
RAT	8.50	118.7	±0.1	645	±13	6804	±137	1235.1	±2.7	2.2415	±0.0044	228 149	±1397	228 102	±1397	2351	±11	228 036	±1397
RAT	9.75	83.8	±0.1	1188	±24	2542	±51	1200.3	±2.3	2.1862	±0.0052	223 677	±1510	223 550	±1511	2256	±11	223 484	±1511
RAT	13.50	85.7	±0.1	1269	±25	2389	±48	1135.8	±2.1	2.1465	±0.0037	232 313	±1265	232 178	±1267	2187	±9	232 112	±1267
RAT	14.00	85.5	±0.1	284	±6	10 808	±221	1156.0	±1.9	2.1804	±0.0031	235 607	±1093	235 576	±1093	2247	±8	235 505	±1093
RAT	15.00	54.6	±0.1	584	±12	3312	±67	1120.2	±2.1	2.1475	±0.0035	237 779	±1277	237 680	±1278	2191	±9	237 616	±1278
RAT	15.25	70.9	±0.1	1169	±23	2108	±42	1085.7	±1.6	2.1074	±0.0036	237 367	±1258	237 213	±1261	2121	±8	237 142	±1261
RAT	15.50	76.1	±0.1	4946	±99	519	±10	1009.5	±2.0	2.0490	±0.0038	246 517	±1518	245 888	±1574	2021	±10	245 822	±1574
RAT	16.00	75.3	±0.1	2113	±42	1159	±23	925.9	±2.0	1.9725	±0.0033	253 671	±1568	253 388	±1578	1893	±9	253 326	±1578
RAT	16.50	56.9	±0.0	457	±9	4187	±85	926.5	±1.7	2.0405	±0.0039	282 375	±2087	282 297	±2087	2055	±13	282 226	±2087
RAT	17.00	67.7	±0.1	75	±2	29 556	±732	887.3	±1.7	1.9982	±0.0034	284 836	±1946	284 824	±1946	1982	±12	284 753	±1946
RAT	17.70	71.3	±0.1	110	±2	20 978	±466	859.2	±1.6	1.9700	±0.0036	287 778	±2109	287 761	±2109	1935	±12	287 690	±2109
RAT	18.25	78.5	±0.1	654	±13	3843	±77	834.4	±2.0	1.9399	±0.0038	287 767	±2405	287 682	±2404	1879	±14	287 620	±2404
RAT	20.00	90.0	±0.1	445	±9	6121	±124	738.5	±2.2	1.8340	±0.0036	293 865	±2657	293 810	±2656	1692	±14	293 744	±2656
RAT	23.00	94.2	±0.1	657	±13	4069	±82	636.2	±1.8	1.7211	±0.0034	301 956	±2809	301 874	±2808	1491	±13	301 812	±2808
RAT	24.00	79.5	±0.1	28	±1	77 872	±3369	571.6	±1.4	1.6549	±0.0027	312 266	±2597	312 260	±2597	1380	±11	312 189	±2597
RAT	26.00	80.5	±0.1	55	±2	38 662	±1081	528.9	±1.9	1.6075	±0.0028	317 242	±3246	317 232	±3246	1295	±13	317 166	±3246
RAT	28.00	96.1	±0.1	230	±5	10 923	±221	515.8	±1.9	1.5882	±0.0034	314 689	±3633	314 657	±3632	1253	±14	314 595	±3632
RAT	28.75	87.6	±0.1	686	±14	3275	±66	486.5	±1.7	1.5556	±0.0035	318 254	±3778	318 148	±3776	1194	±13	318 086	±3776
RAT	29.50	103.9	±0.1	172	±4	15 358	±318	476.0	±2.0	1.5440	±0.0030	319 752	±3689	319 729	±3689	1173	±13	319 663	±3689
RAT	32.00	63.9	±0.1	144	±3	11 459	±245	485.3	±1.7	1.5627	±0.0030	326 523	±3661	326 492	±3661	1219	±13	326 426	±3661
RAT	32.75	89.9	±0.1	153	±3	15 552	±315	520.6	±1.8	1.6073	±0.0039	326 426	±4204	326 404	±4203	1308	±16	326 342	±4203
RAT	34.00	72.7	±0.1	217	±4	9021	±186	535.3	±1.9	1.6372	±0.0033	337 484	±4138	337 446	±4137	1387	±17	337 380	±4137
RAT	35.00	81.5	±0.1	162	±3	13 893	±281	573.2	±1.8	1.6805	±0.0036	332 647	±3944	332 622	±3943	1465	±17	332 560	±3943
RAT	35.75	81.9	±0.1	100	±2	22796	±523	576.1	±1.4	1.6865	±0.0030	334 834	±3324	334 818	±3323	1482	±14	334 747	±3323
RAT	36.60	90.5	±0.1	470	±10	5671	±115	655.1	±1.6	1.7878	±0.0027	335 551	±2982	335 493	±2981	1688	±15	335 422	±2981
RAT	36.75	80.7	±0.1	195	±4	11499	±240	573.5	±1.8	1.6833	±0.0034	334 990	±3912	334 960	±3911	1476	±17	334 894	±3911
RAT	37.00	99.5	±0.1	428	±9	7265	±147	731.9	±1.5	1.8963	±0.0030	344 621	±3138	344 576	±3137	1935	±18	344 505	±3137
RAT	37.25	85.1	±0.1	572	±12	5019	±102	838.0	±2.2	2.0452	±0.0041	355 336	±4289	355 275	±4288	2284	±28	355 209	±4288
RAT	37.50	100.9	±0.1	556	±11	6141	±124	845.7	±1.6	2.0529	±0.0031	353 380	±3159	353 330	±3158	2292	±21	353 259	±3158
RAT	38.50	122.2	±0.1	113	±2	35121	±759	768.4	±1.8	1.9654	±0.0028	365 001	±3564	364 990	±3564	2152	±22	364 924	±3564
RAT	39.00	134.4	±0.1	59	±2	71 303	±1884	712.5	±1.5	1.9010	±0.0031	373 880	±4055	373 874	±4055	2047	±24	373 803	±4055
RAT	40.10	151.9	±0.2	59	±2	80 965	±2468	716.0	±1.9	1.9038	±0.0036	372 020	±4716	372 014	±4716	2046	±28	371 948	±4716
RAT	45.00	146.9	±0.2	53	±2	86 817	±2581	723.2	±2.0	1.9102	±0.0033	368 865	±4477	368 860	±4477	2048	±27	368 794	±4477
RAT	47.00	118.5	±0.1	45	±1	81924	±2460	716.5	±2.1	1.9001	±0.0035	367 292	±4708	367 287	±4708	2020	±28	367 221	±4708
RAT	48.50	117.5	±0.1	183	±4	20120	±425	712.1	±1.6	1.9027	±0.0044	376 488	±5495	376 472	±5494	2060	±32	376 401	±5494
RAT	50.00	92.8	±0.1	52	±2	55 752	±1711	709.6	±2.5	1.9067	±0.0049	384 890	±7090	384 883	±7090	2103	±43	384 817	±7090
RAT	50.70	70.3	±0.0	41	±1	53 378	±1862	709.7	±1.9	1.9042	±0.0037	381 728	±5194	381 721	±5194	2084	±31	381 650	±5194
RAT	51.50	86.0	±0.1	258	±5	10 410	±211	707.5	±2.0	1.8948	±0.0033	374 408	±4678	374 378	±4677	2035	±27	374 314	±4677
VALL 2	0.20	1294.6	±3.1	41	±1	452 066	±15 597	108.8	±2.0	0.8697	±0.0025	159 998	±1252	159 997	±1252	171	±3	159 931	±1252
VALL 2	1.80	342.8	±0.6	12	±0	485 542	±11 926	39.1	±1.7	1.0199	±0.0030	377 308	±11 561	377 304	±11 561	113	±6	377 242	±11561
VALL 2	4.30	289.3	±0.4	28	±1	170 650	±5044	32.0	±1.5	1.0152	±0.0018	392 841	±9902	392 835	±9902	97	±5	392 769	±9902
VALL 2	5.50	334.2	±0.5	4	±1	1 295 999	±278 065	28.8	±1.7	1.0207	±0.0017	436 721	±15 916	436 716	±15 915	99	±7	436 650	±15 915
VALL 2	7.00	315.9	±0.4	23	±1	230 927	±13 011	31.1	±1.5	1.0199	±0.0021	416 922	±13 354	416 916	±13 353	101	±6	416 850	±13 353
VALL 2	7.60	284.5	±0.4	10	±1	503 033	±40 961	35.3	±1.7	1.0281	±0.0018	429 141	±14 893	429 136	±14 893	118	±8	429 070	±14 893
VALL 2	8.10	372.4	±0.6	19	±1	334 429	±20 523	40.4	±1.8	1.0395	±0.0020	454 126	±19 373	454 119	±19 372	145	±10	454 053	±19 372
VALL 2	8.60	246.9	±0.3	36	±1	118 137	±4037	39.7	±1.5	1.0416	±0.0020	474 894	±21 176	474 883	±21 175	151	±11	474 817	±21 175
VALL 2	9.00	770.8	±1.8	10	±1	1 321 617	±104 976	31.0	±2.0	1.0321	±0.0026	494 581	±34 732	494 572	±34 730	125	±15	494 506	±34 730
VALL 2	12.00	811.2	±2.3	56	±2	247 280	±6969	25.4	±2.6	1.0284	±0.0033	540 121	±73 096	540 107	±73 086	117	±28	540 041	±73 086
VALL 2	15.60	211.6	±0.2	24	±1	148 538	±6320	25.4	±1.5	1.0246	±0.0019	495 996	±26 282	495 984	±26 280	103	±10	495 918	±26 280
VALL 2	18.00	335.5	±0.4	29	±1	194 361	±7398	25.1	±1.5	1.0260	±0.0020	514 267	±32 267	514 255	±32 264	107	±12	514 189	±32 264
VALL 2	20.30	348.6	±0.6	11	±1	549 206	±32 644	23.9	±1.5	1.0251	±0.0033	523 624	±48 562	523 612	±48 557	105	±16	523 550	±48 557

U decay constants: $\lambda 238 = 1.55125 \times 10^{-10}$ (Jaffey et al., 1971) and $\lambda 234 = 2.82206 \times 10^{-6}$ (Cheng et al., 2013). Th decay constant: $\lambda 230 = 9.1705 \times 10^{-6}$ (Cheng et al., 2013). [a] $\delta^{234}U = ([^{234}U / ^{238}U]_{activity} - 1) \times 1000$. [b] $\delta^{234}U_{initial}$ was calculated based on ^{230}Th age (T), i.e., $\delta^{234}U_{initial} = \delta^{234}U_{measured} \times e^{\lambda 234 \times T}$. Corrected ^{230}Th ages assume the initial ^{230}Th / ^{232}Th atomic ratio of $4.4 \pm 2.2 \times 10^{-6}$. Those are the values for a material at secular equilibrium, with the bulk Earth ^{232}Th / ^{238}U value of 3.8. The errors are arbitrarily assumed to be 50 %. [c] BP stands for "Before Present", where the "Present" is defined as the year 1950 AD.

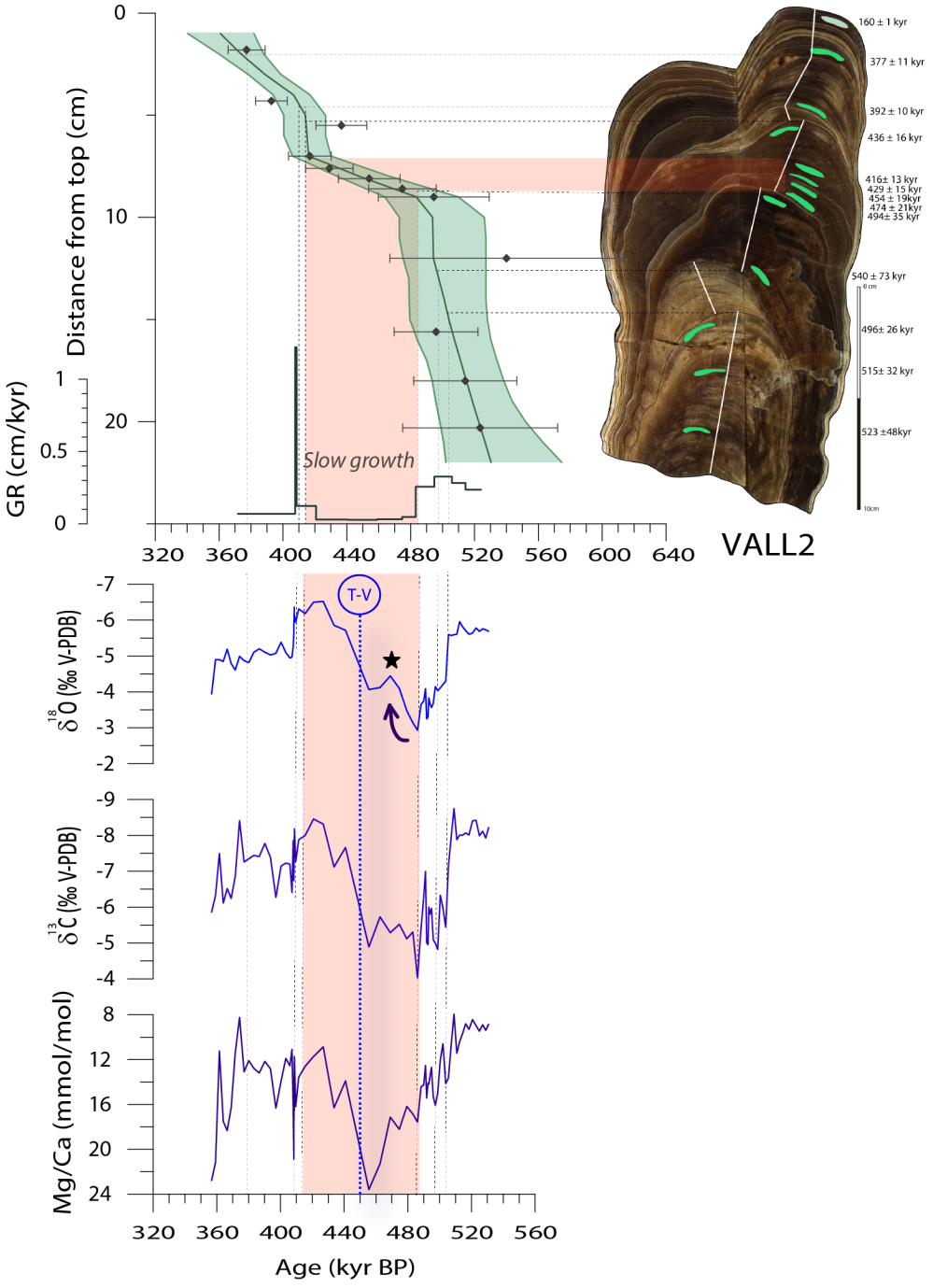

Figure A1. VALL 2 speleothem age model acquired by StalAge (dark blue line) and the original U / Th dates (dark blue dots), plotted with the associated errors (error bars and green area). The VALL 2 growth rates are shown in dark green. On the right, there is the speleothem image with the position of the sampled radiometric dates used for the age model and the growth axis path used for the geochemical analyses (white line). In the lower panel the $\delta^{18}O$, $\delta^{13}C$, and Mg / Ca results with reversal axes. The pink bar highlights a slow growth rate and the dashed grey line points to major color and growth axis direction changes in the speleothem.

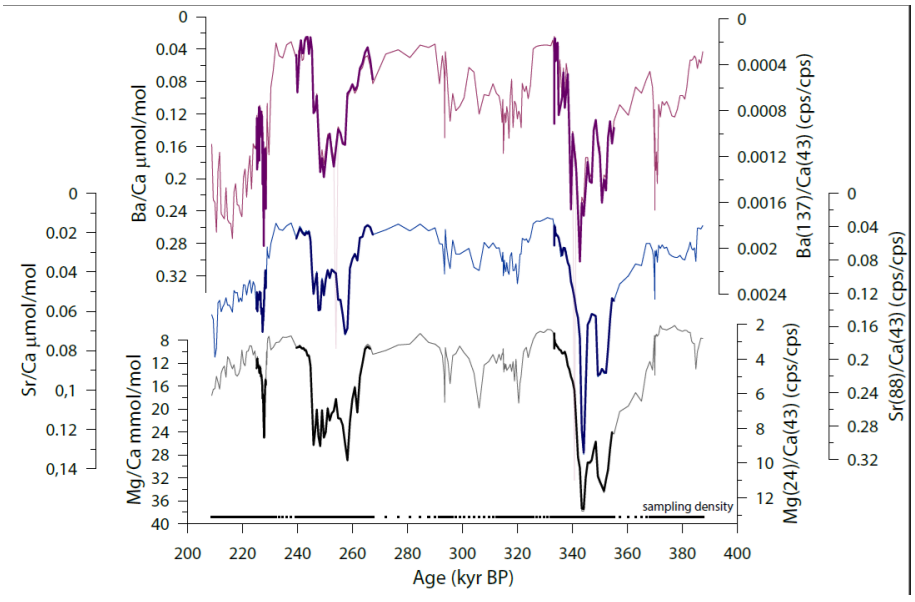

Figure A2. RAT Mg / Ca ratios compared with Sr / Ca and Ba / Ca ratios in counts per second (right axes) and the calculated mmol mol^{-1} and µmol mol^{-1} values (left axes).

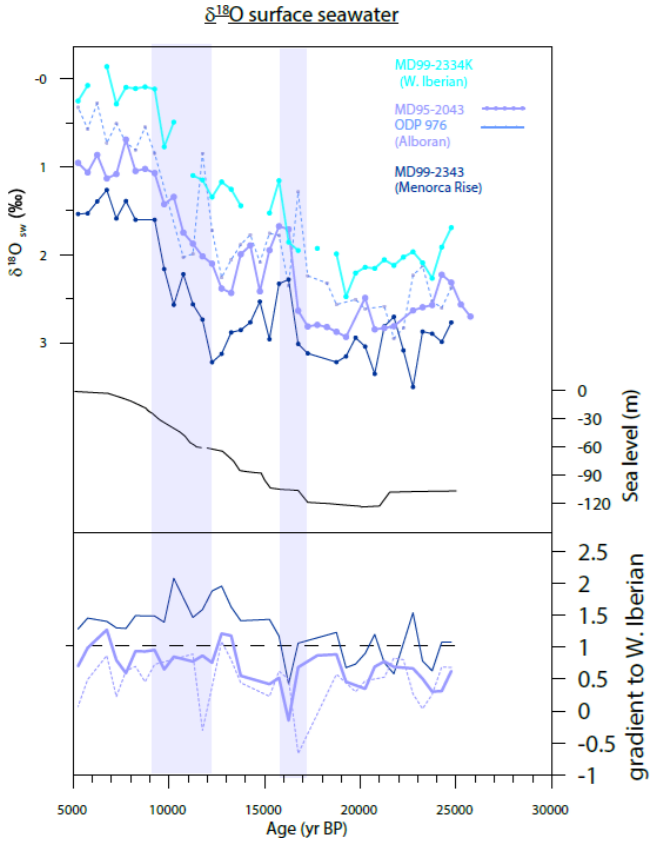

Figure A3. Transmission of the seawater isotopic signal from the North Atlantic to the Mediterranean Sea along the TI modified from Stoll et al. (2022). The $\delta^{18}O_{sw}$ values from paired Mg / Ca and $\delta^{18}O_{plank}$ decline along the deglaciation, with two well-recognized major freshening steps, where one is abrupt at around 16 ka, and the other more gradual from about 12 to 10 ka (vertical blue bars). These freshening events were recorded synchronously and with a similar magnitude in different sediment records from three different locations. The core MD99-2334K from the western Iberian Margin in the North Atlantic (Skinner and Shackleton, 2006) and two sediment cores from the Alboran Sea in the western Mediterranean (Català et al., 2019), with both close to the ODP 977 site, as well as the MD99-2343 core from the Balearic Sea (Català et al., 2019). Sea level rise from Lambeck et al. (2014). In the bottom panel is the gradient of the isotopic signal between the Alboran Sea or the Balearic Sea against the west. The Iberian record shows the characteristic enrichment of the seawater throughout the Mediterranean Sea, with probably higher evaporative processes in the Menorca rise leading to even heavier values in this basin.

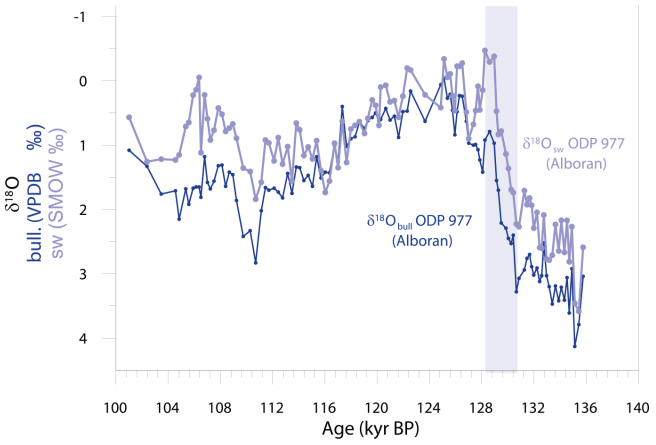

Figure A4. Comparison between the *G. bulloides* $\delta^{18}O_{plank}$ of the ODP 977 site and the $\delta^{18}O_{sw}$ signal obtained by removing the temperature effect using the derived SST Mg / Ca also measured in *G. bulloides* of the same sediment core along glacial termination II (Torner et al., 2019). The maximum rate of freshening along deglaciation coincides in both records as rapid negative $\delta^{18}O$ anomalies and is highlighted by a blue bar.

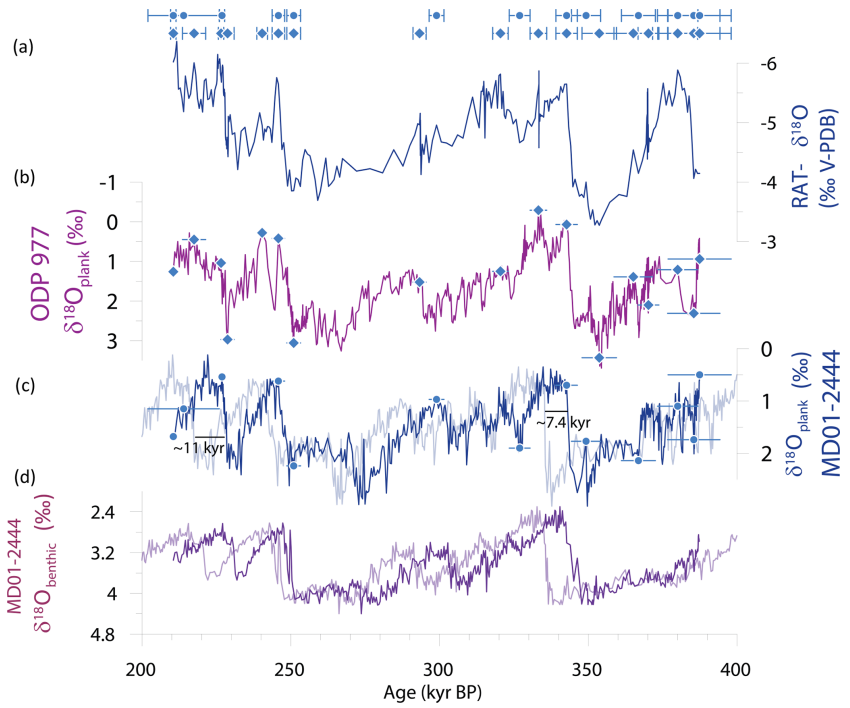

Figure A5. Marine sediment tuning strategy using the RAT age model. At the top, blue circles and diamonds indicate the tie points used for chronological alignment with the speleothem errors associated according to the RAT δ^{18}O record. The ODP 977 δ^{18}O record on the RAT speleothem chronology is in the middle. At the bottom are the MD01-2444 planktic and benthic δ^{18}O records on the RAT speleothem chronology and with the original chronology in light color (Tzedakis et al., 2018).

Data availability. The RAT speleothem data presented in this study will be shared upon request and will be presented for inclusion in the subsequent version of SISAL database.

Author contributions. JT and IC designed and conceptualized the study. JT conducted measurements and analyzed the results. AM and HS provided scientific guidance. JJF coordinated the fieldwork in Mallorca. HC and RLE provided laboratory facilities and funding for U / Th measurements. FJS and JOG provided resources and interpretation of marine core ODP 977. JT was responsible for writing the original draft, while all authors contributed to the discussion and interpretations of the final paper.

Competing interests. The contact author has declared that none of the authors has any competing interests.

Disclaimer. Publisher's note: Copernicus Publications remains neutral with regard to jurisdictional claims made in the text, published maps, institutional affiliations, or any other geographical representation in this paper. While Copernicus Publications makes every effort to include appropriate place names, the final responsibility lies with the authors.

Acknowledgements. Judit Torner and Isabel Cacho acknowledge the financial support from the Catalan Government Grups de Recerca Consolidats (grant no. 2021 SGR 01195). The authors are grateful to Maite Romero and Joaquim Perona from CCiTUB for laboratory support. The authors thank Marc Cerdà for his collaboration with the design of the maps. The authors extend their thanks to Pedro Arnau from Can Saura – Museu Municipal de Ciutadella, Toni Merino, and other members of the Societat Espeleològica Balear for their field support during cave sampling. Isabel Cacho is grateful to the ICREA Academia program from the Generalitat de Catalunya. The authors thank the anonymous reviewers for their valuable comments and discussions which greatly enhanced this work.

Financial support. This research has been supported by the Agencia Estatal de Investigación of the Ministerio de Ciencia e Innovación, which funded the research projects OPERA CTM2013-48639-C2-1-R, CHIMERA CTM2016-75411-R, TRANSMOW PID2019-105523RB-I00, and the PID2020-112720GB-I00. It has also received funding from the European Research Council (ERC) Consolidation Grant (grant no. 683237-TIMED), the ICREA Academia program from the Generalitat de Catalunya, and the Catalan Government Grups de Recerca Consolidats (grant no. 2021 SGR 01195).

Review statement. This paper was edited by Christo Buizert and reviewed by two anonymous referees.

References

Azibeiro, L. A., Sierro, F. J., Capotondi, L., Lirer, F., Andersen, N., González-Lanchas, A., Alonso-Garcia, M., Flores, J. A., Cortina, A., Grimalt, J. O., Martrat, B., and Cacho, I.: Meltwater flux from northern ice-sheets to the mediterranean during MIS 12, Quaternary Sci. Rev., 268, 107108, https://doi.org/10.1016/j.quascirev.2021.107108, 2021.

Barker, S. and Knorr, G.: Millennial scale feedbacks determine the shape and rapidity of glacial termination, Nat. Commun., 14, 2273, https://doi.org/10.1038/s41467-021-22388-6, 2021.

Barker, S., Barker, S., Knorr, G., Edwards, R. L., Parrenin, F., Putnam, A. E., Skinner, L. C., Wolff, E., and Ziegler, M.: 800,000 Years of abrupt climate variability, Science, 334, 347–352, https://doi.org/10.1126/science.1203580, 2011.

Barker, S., Chen, J., Gong, X., Jonkers, L., Knorr, G., and Thornalley, D.: Icebergs not the trigger for North Atlantic cold events, Nature, 520, 333–336, https://doi.org/10.1038/nature14330, 2015.

Barker, S., Knorr, G., Conn, S., Lordsmith, S., and Newman, D.: Early Interglacial Legacy of Deglacial Climate Instability, Paleoceanogr. Paleoclimatol., 2, 1455–1475, https://doi.org/10.1029/2019PA003661, 2019.

Bar-Matthews, M., Ayalon, A., Kaufman, A., and Wasserburg, G.: The Eastern Mediterranean paleoclimate as a reflection of region events: Soreq Cave, Isr. Earth Planet. Sci. Lett., 166, 85–95, https://doi.org/10.1016/S0012-821X(98)00275-1, 1999.

Bar-Matthews, M., Ayalon, M. and Kaufman, A:. Timing and hydrological conditions of Sapropel events in the Eastern Mediterranean, as evident from speleothems, Soreq cave, Israel, Chem. Geol., 169, 145–156, https://doi.org/10.1016/S0009-2541(99)00232-6, 2000.

Bar-Matthews, M., Ayalon, A., Gilmour, M., Matthews, A., and Hawkesworth, C. J.: Sea – land oxygen isotopic relationships from planktonic foraminifera and speleothems in the Eastern Mediterranean region and their implication for paleorainfall during interglacial intervals, Geochim. Cosmochim. Acta, 67, 3181–3199, 2003.

Bartolomé, M., Moreno, A., Sancho, C., Stoll, H. M., Cacho, I., Spötl, C., Belmonte, Á., Edwards, R. L., Cheng, H., and Hellstrom, J. C.: Hydrological change in Southern Europe responding to increasing North Atlantic overturning during Greenland Stadial 1, P. Natl. Acad. Sci. USA, 112, 6568–6572, https://doi.org/10.1073/pnas.1503990112, 2015.

Boers, N.: Observation-based early-warning signals for a collapse of the Atlantic Meridional Overturning Circulation, Nat. Clim. Chang., 11, 680–688, https://doi.org/10.1038/s41558-021-01097-4, 2021.

Cacho, I., Grimalt, J. O., Pelejero, C., Canals, M., Sierro, F. J., Flores, J. A., and Shackleton, N.: Dansgaard-Oeschger and Heinrich event imprints in Alboran Sea paleotemperatures, Paleoceanography, 14, 698–705, https://doi.org/10.1029/1999PA900044, 1999.

Cai, Y., Fung, I. Y., Edwards, R. L., An, Z., Cheng, H., Lee, J., Tan, L., and Shen, C. C., Wang, X., Day, J. A., Zhou, W., Kelly, M. J., and Chiang, J. C. H.: Variability of stalagmite-inferred Indian monsoon precipitation over the past 252 000 y, P. Natl. Acad. Sci. USA, 11210, 2954–2959, https://doi.org/10.1073/pnas.1424035112, 2015.

Català, A., Cacho, I., Frigola, J., Pena, L. D., and Lirer, F.: Holocene hydrography evolution in the Alboran Sea: a multi-record and multi-proxy comparison, Clim. Past, 15, 927–942, https://doi.org/10.5194/cp-15-927-2019, 2019.

Cheng, H., Edwards, R. L., Wang, Y., Kong, X., Ming, Y., Kelly, M. J., Wang, X., and Gallup, C. D.:. A penultimate glacial monsoon record from Hulu Cave and two-phase glacial terminations, Geology 34, 217–220, 2006.

Cheng, H., Edwards, R. L., Broecker, W. S., Denton, G. H., Kong, X., Wang, Y., Zhang, R., and Wang, X.: Ice Age Terminations, Science 326, 248–252,, 2009.

Cheng, H., Sinha, A., Wang, X., Cruz, F. W., and Edwards, R. L.: The global paleomonsoon as seen through speleothem records from Asia and the Americas, Clim. Dyn., 39, 1045–1062, https://doi.org/10.1007/s00382-012-1363-7, 2012.

Cheng, H., Edwards, R. L., Chuan-Chou, S., Polyak, V. J., Asmerom, Y., Woodhead, J., Hellstrom, J., Yongjin, W., Xinggong, K., Spotl, C., Xianfeng, W., and Alexander Jr., E. C.: Improvements in 230Th dating, 230Th and 234U half-life values, and U-Th isotopic measurements by multi-collector inductively coupled plasma mass spectrometry, Earth Planet. Sc. Lett., 371–372, 82–91, https://doi.org/10.1016/j.epsl.2013.04.006, 2013.

Cheng, H., Spötl, C., Breitenbach, S. F. M., Sinha, A., Wassenburg, J. A., Jochum, K. P., Scholz, D., Li, X., Yi, L., Peng, Y., Lv, Y., Zhang, P., Votintseva, A., Loginov, V., Ning, Y., Kathayat, G., and Edwards, R. L.: Climate variations of Central Asia on orbital to millennial timescales, Sci. Rep., 5, 1–11, https://doi.org/10.1038/srep36975, 2016.

Clark, P. U., Shakun, J. D., Baker, P. A., Bartlein, P. J., Brewer, S., Brook, E., Carlson, A. E., Cheng, H., Kaufman, D. S., Liu, Z., Marchitto, T. M., Mix, A. C., Morrill, C., Otto-Bliesner, B. L., Pahnke, K., Russell, J. M., Whitlock, C., Adkins, J. F., Blois, J. L., Clark, J., Colman, S. M., Curry, W. B., Flower, B. P., He, F., Johnson, T. C., Lynch-Stieglitz, J., Markgraf, V., McManus, J., Mitrovica, J. X., Moreno, P. I., and Williams, J. W.: Global climate evolution during the last deglaciation, P. Natl. Acad. Sci. USA, 109, E1134–E1142, https://doi.org/10.1073/pnas.1116619109, 2012

Columbu, A., Spötl, C., De Waele, J., Yu, T. L., Shen, C. C., and Gázquez, F.: A long record of MIS 7 and MIS 5 climate and environment from a western Mediterranean speleothem (SW Sardinia, Italy), Quaternary Sci. Rev., 220, 230–243, https://doi.org/10.1016/j.quascirev.2019.07.023, 2019.

Coplen, T. B.: New guidelines for reporting stable hydrogen, carbon, and oxygen isotope-ratio data, Geochim. Cosmochim. Acta, 60, 3359–3360, https://doi.org/10.1016/0016-7037(96)00263-3, 1996.

Cruz, F. W., Burns, S. J., Karmann, I., Sharp, W. D., Vuille, M., Cardoso, A. O., Ferrari, J. A., Silva Dias, P. L., and Viana, O.: Insolation-driven changes in atmospheric circulation over the past 116,000 years in subtropical Brazil, Nature, 434, 63–66, 2005.

Cruz, F. W., Vuille, M., Burns, S. J., Wang, X., Cheng, H., Werner, M., Lawrence Edwards, R., Karmann, I., Auler, A. S., and

Nguyen, H.: Orbitally driven east–west antiphasing of South American precipitation, Nat. Geosci., 2, 210–214, 2009.

Dorale, J. A., Onac, B. P., Fornós, J. J., Ginés, J., Ginés, A., Tuccimei, P., and Peate, D. W.: Sea-level highstand 81,000 years ago in mallorca, Science, 327, 860–863, https://doi.org/10.1126/science.1181725, 2010.

Drysdale, R. N., Zanchetta, G., Hellstrom, J. C., Fallick, A. E., Zhao, J. X., Isola, I., and Bruschi, G.: Palaeoclimatic implications of the growth history and stable isotope δ^{18}O and δ^{13}C. Geochemistry of a Middle to Late Pleistocene stalagmite from central-western Italy, Earth Planet. Sc. Lett., 227, 215–229, https://doi.org/10.1016/j.epsl.2004.09.010, 2004.

Drysdale, R. N. Hellstrom, J. C., Zanchetta, G., Fallick, A. E., Sánchez-Goñi, M. F., and Couchoud, I.: Evidence for obliquity forcing of glacial termination II, Science, 3255947, 1527–1531, https://doi.org/10.1126/science.1170371, 2009.

Dumitru, O. A., Forray, F. L., Fornós, J. J., Ersek, V., and Onac, B. P.: Water isotopic variability in Mallorca: a path to understanding past changes in hydroclimate, Hydrol. Process., 31, 104–116, https://doi.org/10.1002/hyp.10978, 2017.

Dumitru, O. A., Onac, B. P., Polyak, V. J., Wynn, J. G., Asmerom, Y., and Fornós, J. J.: Climate variability in the western Mediterranean between 121 and 67 ka derived from a Mallorcan speleothem record, Palaeogeogr. Palaeocl. 506, 128–138, https://doi.org/10.1016/j.palaeo.2018.06.028, 2018.

Fairchild, I. J., Borsato, A., Tooth, A. F., Frisia, S., Hawkesworth, C. J., Huang, Y., McDermott, F., and Spiro, B.: Controls on trace element Sr-Mg. compositions of carbonate cave waters: Implications for speleothem climatic records, Chem. Geol., 166, 255–269, https://doi.org/10.1016/S0009-2541(99)00216-8, 2000.

García-Alix, A., Camuera, J., Ramos-Román, M. J., Toney, J. L., Sachse, D., Schefub, E., Jimenez-Moreno, G., Jiménez-Espejo, F. J., López-Avilés, A., Anderson, R. S., and Yanes, Y.: Paleohydrological dynamics in the Western Mediterranean during the last glacial cycle, Global Planet. Change, 202, 103527, https://doi.org/10.1016/j.gloplacha.2021.103527, 2021.

Genty, D., Verheyden, S., and Wainer, K.: Speleothem records over the last interglacial. Investigating Past Interglacials, PAGES news, 21, 1–2, 2013.

Gimeno, L., Nieto, R., Trigo, R. M., Vicente-Serrano, S. M., and López-Moreno, J. I.: Where does the Iberian Peninsula moisture come from? An answer based on a Lagrangian approach, J. Hydrometeorol., 11, 421–436, https://doi.org/10.1175/2009JHM1182.1, 2010.

Gonzalez-Mora, B., Sierro, F. J., and Schönfeld, J.: Temperature and stable isotope variations in different water masses from the Alboran Sea (Western Mediterranean) between 250 and 150 ka, Geochem. Geophys. Geosyst., 9, Q10016 https://doi.org/10.1029/2007GC001906, 2008.

Grant, K. M., Rohling, E. J., Bar-Matthews, M., Ayalon, A., Medina-Elizalde, M., Bronk Ramsey, C., Satow, C., and Roberts, A. P.: Rapid coupling between ice volume and polar temperature over the past 150 kyr, Nature, 491, 744–747, https://doi.org/10.1038/nature11593, 2012.

Grant, K. M., Grimm, R., Mikolajewicz, U., Marino, G., Ziegler, M., and Rohling, E. J.: The timing of Mediterranean sapropel deposition relative to insolation, sea-level and African monsoon changes, Quaternary Sci. Rev., 140, 125–141, https://doi.org/10.1016/j.quascirev.2016.03.026, 2016.

Hellstrom, J., McCulloch, M., and Stone, J.: A Detailed 31,000-Year Record of Climate and Vegetation Change, from the Isotope Geochemistry of Two New Zealand Speleothems, Quaternary Res., 50, 167–178, https://doi.org/10.1006/qres.1998, 1998.

Hobart, B., Lisiecki, L. E., Rand, D., Lee, T., and Lawrence, C. E.: Late Pleistocene 100-kyr glacial cycles paced by precession forcing of summer insolation, Nat. Geosci., 16, 717–722, https://doi.org/10.1038/s41561-023-01235-x, 2023.

Hodell, D., Crowhurst, S., Skinner, L., Tzedakis, P. C., Margari, V., Channell, J. E. T., Kamenov, G., MacLachlan, S., and Rothwell, G.: Response of Iberian Margin sediments to orbital and suborbital forcing over the past 420 ka, Paleoceanography, 28, 185–199, https://doi.org/10.1002/palo.20017, 2013.

Hodell, D., Lourens, L., Crowhurst, S., Konijnendijk, T., Tjallingii, R., Jiménez-espejo, F., Skinner, L., Shackleton, T., Project, S., Abrantes, F., Acton, G. D., Zarikian, C. A. A., Bahr, A., Balestra, B., Barranco, E. L., Carrara, G., Ducassou, E., Flood, R. D., Flores, J., Furota, S., Grimalt, J., Grunert, P., Hernández-molina, J., Kim, J. K., Krissek, L. A., Kuroda, J., Li, B., Lo, J., Margari, V., Martrat, B., Miller, M. D., Nanayama, F., Nishida, N., Richter, C., Rodrigues, T., Rodríguez-tovar, F. J., Cristina, A., Roque, F., Goñi, M. F. S., Sánchez, F. J. S., Singh, A. D., Sloss, C. R., Stow, D. A. V, Takashimizu, Y., Tzanova, A., Voelker, A., Xuan, C., and Williams, T.: A reference time scale for Site U1385 (Shackleton Site) on the SW Iberian Margin, Global Planet. Change, 133, 49–64, https://doi.org/10.1016/j.gloplacha.2015.07.002, 2015.

Hodell, D. A., Channell, J. E. T., Curtis, J. H., and Romero, O. E.: Onset of "Hudson Strait" Heinrich events in the eastern North Atlantic at the end of the middle Pleistocene transition 640 ka, Paleoceanography, 23, 1–16, https://doi.org/10.1029/2008PA001591, 2008.

Hodell, D. A., Crowhurst, S. J., Lourens, L., Margari, V., Nicolson, J., Rolfe, J. E., Skinner, L. C., Thomas, N. C., Tzedakis, P. C., Mleneck-Vautravers, M. J., and Wolff, E. W.: A 1.5-million-year record of orbital and millennial climate variability in the North Atlantic, Clim. Past, 19, 607–636, https://doi.org/10.5194/cp-19-607-2023, 2023.

Imbrie, J., Hays, J. D., Martinson, D. G., McInteyre, A., Mix, A. C., Morley, J. J., Pisias, N. G., Prell, W. L., and Shackleton, N. J.: The Orbital Theory of Pleistocene Climate: Support from a Revised Chronology of the Marine 18O Record, in: Milankovitch and Climate Part 1, D Reidel Publishing Company, 269–305, 1984.

IPCC: Climate Change 2023: Synthesis Report. Contribution of Working Groups I, II and III to the Sixth Assessment Report of the Intergovernmental Panel on Climate Change, edited by: Core Writing Team, Lee, H., and Romero, J., IPCC, Geneva, Switzerland, 184 pp., https://doi.org/10.59327/IPCC/AR6-9789291691647, 2023.

Jaffey, A. H., Flynn, K. F., Glendenin, L. E., Bentley, W. C., and Essling, A. M.: Precision measurement of half- lives and specific activities of 235U and 238, Phys. Rev., 5, 1889–1906, https://doi.org/10.1103/PhysRevC.4.1889, 1971.

Jian, Z., Wang, Y., Dang, H., Mohtadi, M., Rosenthal, Y., Lea, D. W., Liu, Z., Jin, H., Ye, L., Kuhnt, W., and Wang, X.: Warm pool ocean heat content regulates ocean–continent moisture transport, Nature, 612, 92–99, https://doi.org/10.1038/s41586-022-05302-y, 2022.

Jiménez-Amat, P. and Zahn, R.: Offset timing of climate oscillations during the last two glacial-interglacial transitions connected with large-scale freshwater perturbation, Paleoceanography, 30, 768–788, https://doi.org/10.1002/2014PA002710, 2015.

Kaushal, N., Perez-Mejías, C., and Stoll, H. M.: Perspective on ice age Terminations from absolute chronologies provided by global speleothem records, Clim. Past Discuss. [preprint], https://doi.org/10.5194/cp-2024-37, in review, 2024.

Krklec, K. and Domínguez-Villar, D.: Quantification of the impact of moisture source regions on the oxygen isotope composition of precipitation over Eagle Cave, central Spain, Geoch. Cosm. Acta, 134, 39–54, https://doi.org/10.1016/j.gca.2014.03.011, 2014.

Kutzbach, J. E., Chen, G., Cheng, H., Edwards, R. L., and Liu, Z.: Potential role of winter rainfall in explaining increased moisture in the Mediterranean and Middle East during periods of maximum orbitally-forced insolation seasonality, Clim. Dynam., 42, 1079–1095, https://doi.org/10.1007/s00382-013-1692-1, 2014.

Lambeck, K., Rouby, H., Purcell, A., Sun, Y., and Sambridge, M.: Sea level and global ice volumes from the Last Glacial Maximum to the Holocene, P. Natl. Acad. Sci. USA, 111, 15296–15303, 2014.

Laskar, J., Robutel, P., Joutel, F., Gastineau, M., Correia, A. C. M., and Levrard, B.: A long-term numerical solution for the insolation quantities of the Earth, Astron. Astrophys., 428, 261–285, https://doi.org/10.1051/0004-6361:20041335, 2004.

Lionello, P.: The Climate of the Mediterranean Region: From the Past to the Future, 1st edn., Elsevier Inc, https://doi.org/10.1016/B978-0-12-416042-2.00009-4, 2012.

Lisiecki, L. E. and Raymo, M. E.: A Pliocene-Pleistocene stack of 57 globally distributed benthic δ^{18}O records, Paleoceanography, 201, 1–17, https://doi.org/10.1029/2004PA001071, 2005.

Marino, G., Rohling, E. J., Rodríguez-Sanz, L., Grant, K. M., Heslop, D., Roberts, A. P., Stanford, J. D., and Yu, J.: Bipolar seesaw control on last interglacial sea level, Nature, 522, 197–201, https://doi.org/10.1038/nature14499, 2015.

Marra, F., Rohling, E. J., Florindo, F., Jicha, B., Nomade, S., and Renne, P. R.: Independent ^{40}Ar / ^{39}Ar and ^{14}C age constraints on the last five glacial terminations from the aggradational successions of the Tiber River, Rome (Italy), Earth Planet. Sci. Lett., 449, 105–117, https://doi.org/10.1016/j.epsl.2016.05.037, 2016.

Marra, F., Costantini, L., Buduo, G. M. Di, Florindo, F., Jicha, B. R., Palladino, D. M., and Sottili, G.: Combined glacio-eustatic forcing and volcano-tectonic uplift: Geomorphological and geochronological constraints on the Tiber River terraces in the eastern Vulsini Volcanic District (central Italy), Global Planet. Change, 182, 103009, https://doi.org/10.1016/j.gloplacha.2019.103009, 2019.

Martinson, D. G., Pisias, N. G., Hays, J. D., Imbrie, J., Moore, T. C., and Shackleton, N. J., Age dating and the orbital theory of the ice ages: Development of a high-resolution 0 to 300,000-year chronostratigraphy, Quaternary Res., 27, 1–29, 1987.

Martrat, B., Grimalt, J. O., Lopez-Martínez, C., Cacho, I., Sierro, F. J., Flores, J. A., Zahn, R., Canals, M., Curtis, J. H., and Hodell, D. A.: Abrupt Temperature Changes in the Western Mediterranean over the Past 250,000 Years, Science, 306, 1762–1765, https://doi.org/10.1126/science.1101706, 2004.

Martrat, B., Grimalt, J. O., Shackleton, N. J., De Abreu, L., Hutterli, M. A., and Stocker, T. F.: Four climate cycles of recurring deep and surface water destabilizations on the Iberian margin, Science, 317, 502–507, https://doi.org/10.1126/science.1139994, 2007.

Milankovitch, M.: Kanon der Erdbestrahlung und seine Anwendung auf des Eiszeitenproblem. Special Publication 132, Section of Mathematical and Natural Sciences, vol. 33, p. 633, Royal Serbian Academy of Sciences, Belgrade, Serbia ("Canon of Insolation and the Ice Age Problem") (trans. Israel Program for the US Department of Commerce and the National Science Foundation, Washington, D.C., USA, 1969, and by Zavod za udzbenike i nastavna sredstva in cooperation with Muzej nauke i tehnike Srpske akademije nauka i umetnosti, Belgrade, Serbia, 1998), 1941.

Millán, M. M., Estrela, J., and Miró, J.: Rainfall Components: Variability and Spatial Distribution in a Mediterranean Area (Valencia Region), J. Climate, 18, 2682–2705, https://doi.org/10.1175/JCLI3426.1, 2005.

Moreno, A., Stoll, H., Jiménez-Sánchez, M., Cacho, I., Valero-Garcés, B., Ito, E., and Edwards, R. L.: A speleothem record of glacial 25–11.6 kyr BP. rapid climatic changes from northern Iberian Peninsula, Global Planet. Change, 71, 218–231, https://doi.org/10.1016/j.gloplacha.2009.10.002, 2010.

Moreno, A., Iglesias, M., Azorin-Molina, C., Pérez-Mejías, C., Bartolomé, M., Sancho, C., Stoll, H., Cacho, I., Frigola, J., Osácar, C., Muñoz, A., Delgado-Huertas, A., Bladé, I., and Vimeux, F.: Measurement report: Spatial variability of northern Iberian rainfall stable isotope values – investigating atmospheric controls on daily and monthly timescales, Atmos. Chem. Phys., 21, 10159–10177, https://doi.org/10.5194/acp-21-10159-2021, 2021.

Moseley, G. E., Edwards, R. L., Wendt, K. A., Cheng, H., Dublyansky, Y., Lu, Y., and Boch, R.: Reconciliation of the Devils Hole climate record with orbital forcing, Science, 351, 165–168, 2016.

Nichols, M. D., Xuan, C., Crowhurst, S., Richter, C., Acton, G. D., and Wilson, P. A.: Climate – Induced Variability in Mediterranean Out fl ow to the North Atlantic Ocean During the Late Pleistocene, Paleoceanography and Paleoclimatology, 35, 1–17, https://doi.org/10.1029/2020PA003947, 2020.

Nieto, R., Gimeno, L., Drumond, A., and Hernandez, E.: A Lagrangian identification of the main moisture sources and sinks affecting the Mediterranean area, WSEAS Trans. Env. Dev. 6, 365–374, 2010.

Ochoa, D., Sierro, F. J., Hilgen, F. J., Cortina, A., Lofi, J., Kouwenhoven, T., and Flores, J. A.: Origin and implications of orbital-induced sedimentary cyclicity in Pliocene well-logs of the Western Mediterranean, Mar. Geol., 403, 150–164, https://doi.org/10.1016/j.margeo.2018.05.009, 2018.

Past Interglacials Working Group of PAGES: Interglacials of the last 800,000 years. Rev. Geophys., 54, 162–219, https://doi.org/10.1002/2015RG000482, 2016.

Paillard, D., Labeyric, L., and Yiou, P.: Machintosh program performs time-series analysis, Eos Transactions, AGU 77, 379–379, https://doi.org/10.1029/96EO00259, 1996.

Pérez-Mejías, C., Moreno, A., Sancho, C., Bartolomé, M., Stoll, H., Cacho, I., Cheng, H., and Edwards, R. L., Abrupt climate changes during Termination III in Southern Europe, P. Natl. Acad. Sci. USA, 11438, 10047–10052, https://doi.org/10.1073/pnas.1619615114, 2017.

Rahmstorf, S.: Ocean circulation and climate during the past 120,000 years, Nature, 419, 207–214, https://doi.org/10.1038/nature01090, 2002.

Rohling, E. J., Foster, G. L., Grant, K. M., Marino, G., Roberts, A. P., Tamisiea, M. E., and Williams, F.: Sea-level and deep-sea-temperature variability over the past 5.3 million years, Nature, 508, 477–482, https://doi.org/10.1038/nature13230, 2014.

Rohling, E. J., Marino, G., and Grant, K. M.: Mediterranean climate and oceanography, and the periodic development of anoxic events sapropels, Earth-Sci. Rev., 143, 62–97, https://doi.org/10.1016/j.earscirev.2015.01.008, 2015.

Sánchez-Goñi, M. F., Eynaud, F., Turon, J. L., and Shackleton, N. J.: High resolution palynological record off the Iberian margin: Direct land-sea correlation for the Last Interglacial complex, Earth Planet. Sci. Lett., 171, 123–137, https://doi.org/10.1016/S0012-821X(99)00141-7, 1999.

Sánchez-Goñi, M. F., Landais, A., Fletcher, W. J., Naughton, F., Desprat, S., and Duprat, J.: Contrasting impacts of Dansgaard – Oeschger events over a western European latitudinal transect modulated by orbital parameters, Quaternary Sci. Rev., 27, 1136–1151, https://doi.org/10.1016/j.quascirev.2008.03.003, 2008.

Schicker, I., Radanovics, S., and Seibert, P.: Origin and transport of Mediterranean moisture and air, Atmos. Chem. Phys., 10, 5089–5105, https://doi.org/10.5194/acp-10-5089-2010, 2010.

Scholz, D. and Hoffmann, D. L.: StalAge: An algorithm designed for construction of speleothem age models, Quat. Geoch., 6, 369–382, https://doi.org/10.1016/j.quageo.2011.02.002, 2011.

Shackleton, N. J.: The last interglacial in the marine and terrestrial records, P. Roy. Soc. Lond. B Bio., 1741034, 135–154, 1969.

Shackleton, N. J., Sánchez-Goñi, M. F., Pailler, D., and Lancelot, Y.: Marine isotope substage 5e and the Eemian interglacial, Global Planet. Change, 36, 151–155, https://doi.org/10.1016/S0921-8181(02)00181-9, 2003.

Shen, C., Edwards, R. L., Cheng, H., Dorale, J. A., Thomas, R. B., Moran, S. B., Weinstein, S. E., and Edmonds, H. N.: Uranium and thorium isotopic and concentration measurements by magnetic sector inductively coupled plasma mass spectrometry, Chem. Geol., 185, 165–178, 2002.

Sierro, F. J., Hodell, D. A., Curtis, J. H., Flores, J. A., Reguera, I., Colmenero-Hidalgo, E., Barcena, M. A., Grimalt, J. O., Cacho, I., Frigola, J., and Canals, M.: Impact of iceberg melting on Mediterranean thermohaline circulation during Heinrich events, Paleoceanography, 20, 1–13, https://doi.org/10.1029/2004PA001051, 2005.

Sierro, F. J., Hodell, D. A., Andersen, N., and Azibeiro, L. A.: Mediterranean Over fl ow Over the Last 250 kyr: Freshwater Forcing From the Tropics to the Ice Sheets, Paleoceanography and Paleoclimatology, 35, 1–31, https://doi.org/10.1029/2020PA003931, 2020.

Skinner, L. and Shackleton, N.: Deconstructing Terminations I and II: revisiting the glacioeustatic paradigm based on deep-water temperature estimates, Quaternary Sci. Rev., 25, 3312–3321, 2006.

Spötl, C., Scholz, D., and Mangini, A.: A terrestrial U / Th-dated stable isotope record of the Penultimate Interglacial, Earth Planet. Sc. Lett., 276, 283–292, https://doi.org/10.1016/j.epsl.2008.09.029, 2008.

Stoll, H., Mendez-Vicente, A., Gonzalez-Lemos, S., Moreno, A., Cacho, I., Cheng, H., and Edwards, R. L.: Interpretation of orbital scale variability in mid-latitude speleothem δ^{18}O: Significance of growth rate controlled kinetic fractionation effects, Quaternary Sci. Rev., 127, 215–228, https://doi.org/10.1016/j.quascirev.2015.08.025, 2015.

Stoll, H. M., Müller, W., and Prieto, M.: I-STAL, a model for interpretation of Mg / Ca, Sr / Ca and Ba / Ca variations in speleothems and its forward and inverse application on seasonal to millennial scales, Geochem. Geophys. Geosys., 13, Q09004, https://doi.org/10.1029/2012GC004183, 2012.

Stoll, H. M., Cacho, I., Gasson, E., Sliwinski, J., Kost, O., Iglesias, M., Torner, J., Perez-Mejías, C., Haghipour, N., Cheng, H., Edwards, R. L., and Moreno, A.: Rapid northern hemisphere ice sheet melting during the penultimate deglaciation, Nat. Commun., 13, 3819, https://doi.org/10.1038/s41467-022-31619-3, 2022.

Torner, J., Cacho, I., Moreno, A., Sierro, F. J., Martrat, B., Rodriguez-Lazaro, J., Frigola, J., Arnau, P., Belmonte, Á., Hellstrom, J., Cheng, H., Edwards, R. L., and Stoll, H.: Ocean-atmosphere interconnections from the last interglacial to the early glacial: An integration of marine and cave records in the Iberian region, Quaternary Sci. Rev., 226, 106037, https://doi.org/10.1016/j.quascirev.2019.106037, 2019.

Toucanne, S., Angue Minto'o, C. M., Fontanier, C., Bassetti, M. A., Jorry, S. J., and Jouet, G.: Tracking rainfall in the northern Mediterranean borderlands during sapropel deposition, Quaternary Sci. Rev., 129, 178–195, https://doi.org/10.1016/j.quascirev.2015.10.016, 2015.

Tzedakis, C.: Timing and duration of Last Interglacial conditions in Europe: A chronicle of a changing chronology, Quaternary Sci. Rev., 22, 763–768, https://doi.org/10.1016/S0277-3791(03)00004-0, 2003.

Tzedakis, P. C., Hooghiemstra, H., and Pälike, H.: The last 1.35 million years at Tenaghi Philippon: revised chronostratigraphy and long-term vegetation trends, Quaternary Sci. Rev., 25, 3416–3430, https://doi.org/10.1016/j.quascirev.2006.09.002, 2006.

Tzedakis, P. C., Raynaud, D., McManus, J. F., Berger, A., Brovkin, V., and Kiefer, T.: Interglacial diversity, Nat. Geosci., 2, 751–755, https://doi.org/10.1038/ngeo660, 2009.

Tzedakis, P. C., Wolff, E. W., Skinner, L. C., Brovkin, V., Hodell, D. A., McManus, J. F., and Raynaud, D.: Can we predict the duration of an interglacial?, Clim. Past, 8, 1473–1485, https://doi.org/10.5194/cp-8-1473-2012, 2012.

Tzedakis, P. C., Crucifix, M., Mitsui, T., and Wolff, E. W.: A simple rule to determine which insolation cycles lead to interglacials, Nat. Publ. Gr., 542, 427–432, https://doi.org/10.1038/nature21364, 2017.

Tzedakis, P. C., Drysdale, R. N., Margari, V., Skinner, L. C., Menviel, L., Rhodes, R. H., Taschetto, A. S., Hodell, D. A., Crowhurst, S. J., Hellstrom, J. C., Fallick, A. E., Grimalt, J. O., McManus, J. F., Martrat, B., Mokeddem, Z., Parrenin, F., Regattieri, E., Roe, K., and Zanchetta, G.: Enhanced climate instability in the North Atlantic and southern Europe during the Last Interglacial, Nat. Commun., 9, 4235, https://doi.org/10.1038/s41467-018-06683-3, 2018.

Waelbroeck, C., Kiefer, T., Dokken, T., Chen, M. T., Spero, H. J., Jung, S., Weinelt, M., Kucera, M., and Paul, A.: Constraints on surface seawater oxygen isotope change between the Last Glacial Maximum and the Late Holocene, Quaternary Sci. Rev., 105, 102–111, https://doi.org/10.1016/j.quascirev.2014.09.020, 2014.

Wagner, B., Vogel, H., Francke, A., Friedrich, T., Donders, T., Lacey, J. H., Leng, M. J., Regattieri, E., Sadori, L.,

Wilke, T., Zanchetta, G., and Albrecht, C.: monsoons during the past 1.36 million years, Nature, 573, 256–260, https://doi.org/10.1038/s41586-019-1529-0, 2019.

Wang, C.: A unified oscillator model for the El Niño-Southern Oscillation, J. Climate, 14, 98–115, 2001.

Wendt, K. A., Li, X., Edwards, R. L., Cheng, H., and Spötl, C.: Precise timing of MIS 7 substages from the Austrian Alps, Clim. Past, 17, 1443–1454, https://doi.org/10.5194/cp-17-1443-2021, 2021.

Yuan, D., Cheng, H., Edwards, R. L., Dykoski, C. A., Kelly, M. J., Zhang, M., Qing, J., Lin, Y., Wang, Y., Wu, J., Dorale, J. A., An, Z., and Cai, Y.: Timing, Duration, and Transitions of the Last Interglacial Asian Monsoon, Science, 304, 575–578, 2004.